Hindawi
Mathematical Problems in Engineering
Volume 2018, Article ID 1512825, 27 pages
https://doi.org/10.1155/2018/1512825

Research Article

Analysis of the Spatial Vibration of Nonprismatic Arches by Means of Recurrence Relations for the Coefficients of the Chebyshev Series Expansion of the Solution

P. Ruta [1] and M. Meissner [2]

[1] *The Faculty of Civil Engineering, Wrocław University of Science and Technology, Wrocław, Poland*
[2] *The Faculty of Environmental Engineering and Geodesy, Wrocław University of Environmental and Life Sciences, Wrocław, Poland*

Correspondence should be addressed to P. Ruta; piotr.ruta@pwr.edu.pl

Received 29 August 2018; Accepted 9 October 2018; Published 31 December 2018

Academic Editor: Francesco Tornabene

The problem of spatial vibrations, both aperiodically forced and free vibrations, of an arch with an arbitrary distribution of material and geometric parameters is considered. Approximation with Chebyshev series was used to solve a conjugated system of partial differential equations describing the problem. The system of differential equations was solved using an algorithm generating a recursive infinite system of equations, developed by S. Paszkowski in "Numerical applications of Chebyshev polynomials" (in Polish), Warsaw PWN, 1975. Since the coefficients of the obtained system of equations are defined by closed analytical formulas they can be directly used to solve any nonprismatic arch, without it being necessary to solve again the considered problem. The algorithm is highly accurate; i.e., already at a small approximation base it yields results agreeing with exact analytical solutions (obviously for problems in the case of which such solutions can be derived). In order to demonstrate this the eigenfrequencies and eigenvectors obtained for a circular prismatic arch were compared with their precise values determined from the exact analytical solutions. The results yielded by the proposed method were also compared with the results obtained by other methods and by other authors. As an illustration, the proposed method was used to solve a more complex problem, i.e., the problem of the free and aperiodically forced vibrations of a nonprismatic arch with its axis described by a catenary curve. In the example the effect of the lack of cross-sectional symmetry of the arch on the form of the system's spatial free and forced vibrations was analysed.

1. Introduction

Since curved beams are often used in civil, mechanical, and aerospace engineering applications, the analysis of their vibrations is of great practical importance. Being described by a conjugated system of partial differential equations with four or six (when the effect of shearing forces is taken into account) unknown functions, the spatial arch vibration problem is quite complicated. It is particularly difficult to solve when all the system parameters, such as curvature and geometric and material characteristics, are variable.

The arch vibration problem has been investigated by many researchers, as evidenced by the abundant literature on this subject. Most of this literature concerns planar systems in which only in-plane or out-of-plane vibrations occur or spatial systems with separated in-plane and out-of-plane vibrations (vibrations are separated when the "generalized" cross-sectional moment of deviation equals zero). The problem of the free vibration of prismatic arches was examined by, among others, Chidamparam and Leissa [2] and Lee et al. [3]. In Chidamparam and Leissa's paper [2] the problem was solved analytically with and without axial deformability taken into account. Also the effect of a static axial force on the eigenproblem solution by the Galerkin method was examined there. Circular arches with different opening angles were considered, but only to determine the natural frequencies. In paper [3] by Lee et al. the natural vibrations of a rotating curved beam with elastically restrained root were analysed. The differential equations describing the problem were derived using the Hamilton principle. The fundamental solution of the system of the differential equations was obtained using the power series method.

The problem of the free vibration of arches with stepped cross sections was solved, using different methods, by, among others, Huang at al. [4], Kawakami et al. [5], Liu and Wu [1], Shin et al. [6], and Tong et al. [7]. Huang et al. [4] analysed arches with any curvature and any cross section and employed the Frobenius method combined with the dynamic stiffness method to solve the problem. The same method was used by Huang et al. in [8] to solve the free vibration-and-stability problem with shape deformation taken into account. Kawakami et al. in paper [5] solved the eigenproblem using the discrete Green function. Liu and Wu [1] applied the generalized differential quadrature rule (GDQR) to solve the eigenproblem, assuming the arch axis to be inextensible. The numerical examples presented in [1] concerned circular arches with different opening angles and with a constant and stepwise or linearly varying cross section. The obtained nondimensional natural frequencies were compared with the ones determined by other methods by other researchers. The generalized differential quadrature method (GDQM) and the differential transformation method (DTM) were employed by Shin et al. [6]. In paper [7] by Tong et al. a circular arch was analysed and a solution for a prismatic arch was derived, which was then used to solve an arch (considered as a physical approximation) with stepped cross sections. Besides the eigenproblem also the harmonically forced vibration problem was solved there. Karami and Malekzadeh in paper [9] used the differential quadrature method (DQM) to analyse the free vibrations of a circular arch with stepped cross sections. Nieh et al. [10] analytically determined (by the power series method) a stiffness matrix for a prismatic arch, which was then used to solve the free vibration-and-stability problem for an elliptical arch. Eftekhari [11] analysed the vibration of a circular arch with a varying cross-sectional height, applying DQM and Fourier series approximation to solve problems of the free and forced vibrations induced by a moving force.

In many papers the finite element method has been used to analyse vibrations. Krishnan et al. [12] using three different types of finite elements (differing in their number of degrees of freedom) solved the eigenproblem, but for only the first natural frequency. In Raveendranath et al. [13], various types of elements, differing in the degrees of the power polynomials used to approximate the shape function, were developed. The elements were used to solve the vibration problem for a circular prismatic arch. Yang et al. in [14] developed two types of elements, corresponding to two arch models. One of the models took into account the effect of shape deformability and rotary inertia, whereas the other did not, assuming that the arch axis did not deform axially. The shape functions were approximated with power polynomials. The defined finite elements were used to solve many numerical examples (including arches with variable parameters) in which eigenfrequencies and eigenforms were determined. Öztürk et al. [15], using the assumption about arch axial nondeformability and assuming the shape functions in the form of a combination of trigonometric functions and classical polynomials, developed a finite element and employed it to solve the free vibration-and-dynamic stability problem for the arch. An element developed using exact (for the static problem) shape functions (Litewka and Rakowski [16]) was employed in Litewka and Rakowski [17]. The functions, being combinations of trigonometric functions, were further transformed by replacing the trigonometric functions with their expansions into power series and rejecting the higher-order terms. The finite element was used to solve the free vibration problem. Also Zhu and Meguid [18] worked on developing a finite element for the curved beam. A three-node element was defined and used to analyse free vibrations. The results were compared with experimental results. An interesting approach to the solution of the free vibration problem for an arch with discontinuities (additional elastic constraints, mass elements, and stepwise change in curvature), based on wave propagation techniques was presented in Kang et al. [19] and Riedel and Kang [20]. In the latter paper only the discontinuities arising from additional elastic constraints were taken into account. Using the coupled displacement field methodology and coupled shape functions derived from the static equilibrium consideration Ishaquddin et al. [21] developed a curvilinear beam finite element for the Euler-Bernoulli beam and the Timoshenko beam. The designed element is resistant to shear, flexure, and torsion locking. The element was used in an analysis of the circular arch eigenproblem. The computed out-of-plane free vibration frequencies were compared with the analytical solution.

Curved laminated composite beams with constant curvature were considered by Jafari-Taookolaei et al. [22], who analytically solved the eigenproblem, taking delamination into account, and developed a curvilinear finite element. Li et Geudes Soares [23] developed a spectral finite element model based on shear deformation theory. The exact solution of the governing homogeneous differential equations was used as the shape functions. The eigenproblem of a circular laminated arch with a constant cross section was analysed and natural frequencies and eigenforms were determined. Laminated composite and sandwich beams with constant and varying (circular, elliptical, and parabolic) curvature were analysed by Ye, Jin, and Su [24]. A spectral-sampling surface method was developed and applied to the eigenproblem of the curved laminated beam. Sadeghpour et al. [25] analysed a debonded curved sandwich beam. Relevant equations of motion were derived from the Lagrange equation. The Rayleigh-Ritz method was used to discretize the system. The eigenproblem was solved using the Lanczos algorithm. The determined natural frequencies and eigenforms were compared with the results yielded by the finite element method.

Most of the above works on laminated beams focused on the analysis of the effect of lamination on the system's response. The considerations were limited to arches with constant curvature and a cross section invariable along their length.

The work by Yu et al. [26] is an example of an analysis of more complex models, including curved spatial systems. A spatial beam model based on Washizu's static model was analysed. The model was used to investigate the in-plane and out-of-plane vibrations of a circular arch with a triangular cross section. Also the spatial problem was solved and the eigenfrequencies of a helical cylindrical spring were determined. The spatial free vibrations of circular planar arches were analysed in work [27] by Caliò, assuming the

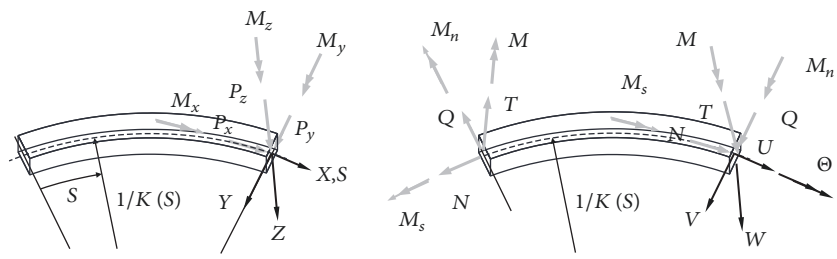

Figure 1: Local coordinate system, external forces, displacements, and internal forces.

differential equations describing the in-plane and out-of-plane vibrations of the arch to be separated. Caliò introduced dynamic stiffness matrices for an arch and a curved-in-plane girder. He solved the eigenproblem using the Wittrick and Williams method. The results obtained as part of a numerical example illustrating the analysis of the vibrations of a spatial system consisting of arch elements were compared with the results yielded by FEM.

The above survey of literature covers papers published in the last ten-twenty years, and so it is obviously incomplete. A wide survey of the earlier papers can be found in, e.g., the review study by Auciello and De Rosa [28]. Nevertheless, even this brief survey of literature shows that most of the research on the vibrations of arches has been limited to solving the eigenproblem and only a few of the papers are devoted to the problem of (usually harmonically) forced vibrations.

The problem was solved using the method previously applied to solve the free vibration problem for the Euler beam in the author's papers [29, 30] and for the Timoshenko beam in [31]. The method is based on the way of approximately solving ordinary linear differential equations by means of Chebyshev series, presented in the monograph by Paszkowski [32]. The way referred to makes it possible to reduce the differential equations to a system of algebraic equations. Unfortunately, the coefficients of the latter equations are combinations of the linear coefficients in the expansions of the initial functions (occurring in the differential equations) and their higher derivatives. An effective algorithm can be developed by transforming the coefficients so that they will contain only the terms of the expansions of the initial functions and not their derivatives. Because of their length and the limited confines of this paper the transformations are not included here. It should be noted that the final solution for the given form of differential equations has a general character and enables ones to solve a system with any geometric and material parameters. Moreover, as demonstrated in this paper and in the earlier papers by the author, the proposed method makes it possible (within the adopted model) to obtain highly accurate solutions.

The use of Chebyshev series to solve structural mechanics problems (and other problems) is a known fact. The series are used owing to, among other things, their good approximation properties. However, to the present authors' knowledge there have been no other works in which the recursive algorithm (see Paszkowski [32]) employed in this paper was used to generate equations enabling the direct determination of the expansion coefficients of the sought functions.

In order to verify the derived formulas, the algorithm was applied to solve two examples. The first one was taken from papers by other authors and used to compare the obtained results with the ones determined by other methods. The eigenproblem was solved in this example. In the second example the problem of the aperiodically forced vibrations of an arch with a varying cross section was analysed. Since in this example the eigentransformation method was employed to solve the aperiodically forced vibration problem, the eigenproblem was solved in the first step. A rectangular pulse and a nonstationary harmonic excitation were assumed as the aperiodic excitation.

2. Problem Formulation

A nonprismatic arch, described in accordance with the Bernoulli-Euler theory, is analysed.

The arch is subjected to time-variable force loads $P_x(S,t)$, $P_y(S,t)$, $P_z(S,t)$ and moment loads $M_x(S,t)$, $M_y(S,t)$, $M_z(S,t)$ (Figure 1). The axis of the arch is a plane curve having length $2a$, defined by parametric equation $\mathbf{r}(s)$, where $s \in \langle -a, a\rangle$.

If the nondimensional variables and functions $x = X/a$, $y = Y/a$, $z = Z/a$, $s = S/a$, $u(s,t) = U(S,t)/a$, $v(s,t) = V(S,t)/a$, $w(s,t) = W(S,t)/a$, and $\vartheta(s,t) = \Theta(S,t)/a$ are introduced, the following system of fourth-order partial differential equations describing the arch vibrations is obtained:

$$\begin{aligned}
&dEA\frac{\partial^2 u}{\partial s^2} + d\frac{\partial EA}{\partial s}\frac{\partial u}{\partial s} - \left(\frac{\partial \kappa}{\partial s}\right)^2 EI_z u - \frac{\partial \kappa}{\partial s} EI_z \frac{\partial^2 v}{\partial s^2} \\
&\quad - d\kappa EA\frac{\partial v}{\partial s} - \left(d\frac{\partial}{\partial s}(\kappa EA) + \frac{\partial \kappa}{\partial s}\kappa^2 EI_z\right) v \\
&\quad - \frac{\partial \kappa}{\partial s} EI_{yz}\frac{\partial^2 w}{\partial s^2} + \kappa\frac{\partial \kappa}{\partial s} EI_{yz}\vartheta = -f\left(p_x + \kappa m_z\right) \\
&\quad + g\rho\frac{\partial^2 u}{\partial t^2},
\end{aligned} \tag{1a}$$

$$\begin{aligned}
&-\frac{\partial \kappa}{\partial s} EI_z \frac{\partial^2 u}{\partial s^2} + \left(d\kappa\overline{EA} - 2\frac{\partial}{\partial s}\left(\frac{\partial \kappa}{\partial s} EI_z\right)\right)\frac{\partial u}{\partial s} \\
&\quad - \left(\frac{\partial^2}{\partial s^2}\left(\frac{\partial \kappa}{\partial s} EI_z\right) + \frac{\partial \kappa}{\partial s}\kappa^2 EI_z\right) u - EI_z\frac{\partial^4 v}{\partial s^4} \\
&\quad - 2\frac{\partial EI_z}{\partial s}\frac{\partial^3 v}{\partial s^3} - \left(\frac{\partial^2 EI_z}{\partial s^2} + 2\frac{\partial^2 \kappa}{\partial s^2} EI_z\right)\frac{\partial^2 v}{\partial s^2}
\end{aligned}$$

$$
\begin{aligned}
&-2\kappa EI_z\frac{\partial v}{\partial s}-\left(d\kappa^2\overline{EA}+\frac{\partial^2}{\partial s^2}\left(\kappa^2EI_z\right)+\kappa^4EI_z\right)v\\
&-EI_{yz}\frac{\partial^4 w}{\partial s^4}-2\frac{\partial EI_{yz}}{\partial s}\frac{\partial^3 w}{\partial s^3}\\
&-\left(\frac{\partial^2 EI_{yz}}{\partial s^2}+\kappa^2EI_{yz}\right)\frac{\partial^2 w}{\partial s^2}+\kappa EI_{yz}\frac{\partial^2\vartheta}{\partial s^2}\\
&+2\frac{\partial}{\partial s}\left(\kappa EI_{yz}\right)\frac{\partial\vartheta}{\partial s}+\frac{\partial^2}{\partial s^2}\left(\kappa^3EI_{yz}+\kappa\frac{\partial^2EI_{yz}}{\partial s^2}\right)\vartheta\\
&=-f\left(p_y+\frac{\partial m_z}{\partial s}\right)+g\rho\frac{\partial^2 v}{\partial t^2},
\end{aligned}
\tag{1b}
$$

$$
\begin{aligned}
&-\frac{\partial\kappa}{\partial s}EI_{yz}\frac{\partial^2 u}{\partial s^2}-2\frac{\partial}{\partial s}\left(\frac{\partial\kappa}{\partial s}EI_{yz}\right)\frac{\partial u}{\partial s}\\
&-\frac{\partial^2}{\partial s^2}\left(\frac{\partial\kappa}{\partial s}EI_{yz}\right)u-EI_{yz}\frac{\partial^4 v}{\partial s^4}-2\frac{\partial EI_{yz}}{\partial s}\frac{\partial^3 v}{\partial s^3}\\
&-\left(\kappa^2EI_{yz}+\frac{\partial^2EI_{yz}}{\partial s^2}\right)\frac{\partial^2 v}{\partial s^2}-2\frac{\partial}{\partial s}\left(\kappa^2EI_{yz}\right)\frac{\partial v}{\partial s}\\
&-\frac{\partial^2}{\partial s^2}\left(\kappa^2EI_{yz}\right)v-EI_y\frac{\partial^4 w}{\partial s^4}-2\frac{\partial EI_y}{\partial s}\frac{\partial^3 w}{\partial s^3}\\
&+\left(\kappa^2GJ_s-\frac{\partial^2EI_y}{\partial s^2}\right)\frac{\partial^2 w}{\partial s^2}+\frac{\partial}{\partial s}\left(\kappa^2GJ_s\right)\frac{\partial w}{\partial s}\\
&+\left(\kappa GJ_s+KEI_y\right)\frac{\partial^2\vartheta}{\partial s^2}\\
&+\left(\frac{\partial}{\partial s}\left(\kappa GJ_s\right)+2\frac{\partial}{\partial s}\left(\kappa EI_y\right)\right)\frac{\partial\vartheta}{\partial s}\\
&=-f\left(q_z+\frac{\partial m_y}{\partial s}\right)+g\rho\frac{\partial^2 w}{\partial t^2},
\end{aligned}
\tag{1c}
$$

$$
\begin{aligned}
&\frac{\partial\kappa}{\partial s}\kappa EI_{yz}u+\kappa EI_{yz}\frac{\partial^2 v}{\partial s^2}+\kappa^3EI_{yz}v\\
&+\left(\kappa GJ_s+\kappa EI_y\right)\frac{\partial^2 w}{\partial s^2}+\frac{\partial}{\partial s}\left(\kappa GJ_s\right)\frac{\partial w}{\partial s}+GJ_s\frac{\partial^2\vartheta}{\partial s^2}\\
&+\frac{\partial GJ_s}{\partial s}\frac{\partial\vartheta}{\partial s}-\kappa^2EI_y\vartheta=-fm_x+gJ_s^m\frac{\partial^2\vartheta}{\partial t^2},
\end{aligned}
\tag{1d}
$$

and the nondimensional internal forces are defined by the following formulas:

(i) the axial forces

$$
\begin{aligned}
n=\frac{N}{P_0}=\frac{1}{f}\Bigg(&dEA\left(\frac{\partial u}{\partial s}-\kappa v\right)\\
&-EI_z\kappa\left(\frac{\partial^2 v}{\partial s^2}+\kappa^2v+\frac{\partial\kappa}{\partial s}u\right)\\
&+EI_{yz}K\left(-\frac{\partial^2 w}{\partial s^2}+\kappa\vartheta\right)\Bigg),
\end{aligned}
\tag{2}
$$

(ii) the bending moments

$$
\begin{aligned}
m=\frac{M}{P_0a}=\frac{1}{f}\Bigg(&EI_z\left(\frac{\partial^2 v}{\partial s^2}+\kappa^2v+\frac{\partial\kappa}{\partial s}u\right)\\
&+EI_{yz}\left(\frac{\partial^2 w}{\partial s^2}-\kappa\vartheta\right)\Bigg),
\end{aligned}
\tag{3}
$$

$$
\begin{aligned}
m_n=\frac{M_y}{P_0a}=\frac{1}{f}\Bigg(&EI_y\left(-\frac{\partial^2 w}{\partial s^2}+\kappa\vartheta\right)\\
&-EI_{yz}\left(\frac{\partial^2 v}{\partial s^2}+\kappa\frac{\partial u}{\partial s}+\frac{\partial\kappa}{\partial s}u\right)\Bigg),
\end{aligned}
\tag{4}
$$

(iii) the shearing forces

$$
q=\frac{Q}{P_0}=-\frac{1}{f}\frac{\partial}{\partial s}\left(EI_z\left(\frac{\partial^2 v}{\partial s^2}+\kappa^2v+\frac{\partial\kappa}{\partial s}u\right)\right)+m_z. \tag{5}
$$

$$
\begin{aligned}
t&=\frac{T}{P_0}\\
&=\frac{1}{f}\frac{\partial}{\partial s}\left(\overline{EI}_y\left(-\frac{\partial^2 w}{\partial s^2}+\kappa\vartheta\right)\right)\\
&\quad+\frac{1}{f}\kappa\left(\overline{GJ}_s\left(\kappa\frac{\partial w}{\partial s}+\frac{\partial\vartheta}{\partial s}\right)\right)+m_n
\end{aligned}
\tag{6}
$$

(iv) the torsional moment

$$
m_s=\frac{M_x}{P_0a}=\frac{1}{f}\left(GJ_s\left(\kappa\frac{\partial w}{\partial s}+\frac{\partial\vartheta}{\partial s}\right)\right), \tag{7}
$$

where $u=u(s,t)$ is a nondimensional displacement tangent to the arch axis, $v=v(s,t)$ and $w=w(s,t)$ are nondimensional displacements perpendicular to the arch axis, $\vartheta=\vartheta(s,t)$ is the angle of twist, $\kappa=\kappa(s)$ is the nondimensional arch curvature, $p_x(s,t)=P_x(S,t)/P_0$, $p_y(s,t)=P_y(S,t)/P_0$, $p_z(s,t)=P_z(S,t)/P_0$, $m_x(s,t)=M_x(S,t)/P_0a$, $m_y(s,t)=M_y(S,t)/P_0a$ $m_z(s,t)=M_z(S,t)/P_0a$ are nondimensional external forces, and the nondimensional material and geometric characteristics are $\rho=\overline{\rho}/\rho_0$, density per unit length, $EA=\overline{EA}/EA_0$, axial stiffness, $EI_y=\overline{EI}_y/EI_0$, $EI_z=\overline{EI}_z/EI_0$, flexural stiffness, E, Young's modulus, $\overline{A}=A(S)$, the cross-sectional area, and $\overline{I}_y=I_y(S)$, $\overline{I}_z=I_z(S)$, $\overline{I}_{yz}=I_{yz}(S)$, the generalized moments of inertia, expressed by the formulas:

$$
\begin{aligned}
\overline{I}_y&=\int_A\frac{Z^2}{1-K(S)Y}dA\\
\overline{I}_z&=\int_A\frac{Y^2}{1-K(S)Y}dA\\
\overline{I}_{yz}&=\int_A\frac{YZ}{1-K(S)Y}dA
\end{aligned}
\tag{8}
$$

The constants in formulas ((1a), (1b), (1c), and (1d))–(7) are

$$
\begin{aligned}
f&=\frac{P_0a^2}{EI_0},\\
d&=\frac{a^2EA_0}{EI_0},\\
f&=\frac{a^4\rho_0}{EI_0},
\end{aligned}
\tag{9}
$$

where parameters ρ_0, EA_0, EI_0, P_0 are reference quantities.

3. Problem Solution

The solution of differential equations system ((1a), (1b), (1c), and (1d)) is sought in the form of Chebyshev series of the first kind

$$\begin{aligned} u(x,t) &= \sum_{l=0}^{\infty}{}' a_l[u]\mathrm{T}_l(x) = \sum_{l=0}^{\infty}{}' u_l(t)\mathrm{T}_l(x), \\ v(x,t) &= \sum_{l=0}^{\infty}{}' a_l[v]\mathrm{T}_l(x) = \sum_{l=0}^{\infty}{}' v_l(t)\mathrm{T}_l(x), \\ w(x,t) &= \sum_{l=0}^{\infty}{}' a_l[w]\mathrm{T}_l(x) = \sum_{l=0}^{\infty}{}' w_l(t)\mathrm{T}_l(x), \\ \vartheta(x,t) &= \sum_{l=0}^{\infty}{}' a_l[\vartheta]\mathrm{T}_l(x) = \sum_{l=0}^{\infty}{}' \vartheta_l(t)\mathrm{T}_l(x), \end{aligned} \tag{10}$$

where $\mathrm{T}_l(x)$ is the l-th Chebyshev polynomial of the 1st kind and $a_l[u]$, $a_l[v]$, $a_l[w]$, and $a_l[\vartheta]$ are unknown coefficients of the expansion of displacement functions u, v, w, ϑ into Chebyshev series, hereafter denoted as u_l, v_l, w_l, ϑ_l.

The method presented in Appendix A and in the author's papers [29–31] will be used to solve the problem. In this method the system of ordinary differential equations is reduced to a recursive infinite system of algebraic equations. If the initial equations are partial differential equations, a system of ordinary differential equation is obtained.

The characteristic feature of this method is that the coefficients of the obtained infinite system of equations are in an analytical form whereby the equations derived in this paper can be used to solve any arch, without it being necessary to transform the initial equations. The high accuracy of the results yielded by proposed method, demonstrated in this paper, is comparable with that of the exact closed analytical solutions.

In order to apply this method to the considered problem let us reduce the system of equations to the matrix form

$$\begin{aligned} &\widehat{\mathbf{P}}_{\mathbf{0}}(s)\,\mathbf{f}^{(4)}(s,t) + \widehat{\mathbf{P}}_{\mathbf{1}}(s)\,\mathbf{f}^{(3)}(s,t) + \widehat{\mathbf{P}}_{2}(s)\,\mathbf{f}^{(2)}(s,t) \\ &\quad + \widehat{\mathbf{P}}_{3}(s)\,\mathbf{f}^{(1)}(s,t) + \widehat{\mathbf{P}}_{4}(s)\,\mathbf{f}(s,t) \\ &= \widehat{\mathbf{P}}(s,t) + \widehat{\mathbf{R}}_{4}(s)\,\ddot{\mathbf{f}}(s,t), \end{aligned} \tag{11}$$

where matrix functions $\widehat{\mathbf{P}}_m(s)$, $m = 0,1,2,3,4$; $\widehat{\mathbf{R}}_4(s)$ and vector $\widehat{\mathbf{P}}(s,t)$ are expressed by the formulas (a simplified form of derivative $f^{(p)}(s) = \partial^p f(s)/\partial s^p$ is used to shorten the notation)

$$\widehat{\mathbf{P}}_0 = \begin{bmatrix} 0 & 0 & 0 & 0 \\ 0 & -EI_z & -EI_{yz} & 0 \\ 0 & -EI_{yz} & -EI_y & 0 \\ 0 & 0 & 0 & 0 \end{bmatrix}, \tag{12a}$$

$$\widehat{\mathbf{P}}_1 = \begin{bmatrix} 0 & 0 & 0 & 0 \\ 0 & -2\left(EI_z\right)^{(1)} & -2\left(EI_{yz}\right)^{(1)} & 0 \\ 0 & -2\left(EI_{yz}\right)^{(1)} & -2\left(EI_y\right)^{(1)} & 0 \\ 0 & 0 & 0 & 0 \end{bmatrix}, \tag{12b}$$

$$\widehat{\mathbf{P}}_2 = \begin{bmatrix} dEA & -\kappa^{(1)}EI_z & -\kappa^{(1)}EI_{yz} & 0 \\ -\kappa^{(1)}EI_z & -\left(EI_z\right)^{(2)} - 2\kappa^2 EI_z & -\kappa^2 EI_{yz} - \left(EI_{yz}\right)^{(2)} & \kappa EI_{yz} \\ -\kappa^{(1)}EI_{yz} & -\kappa^2 EI_{yz} - \left(EI_{yz}\right)^{(2)} & \kappa^2 GJ_s - \left(EI_y\right)^{(2)} & \kappa GJ_s + \kappa EI_y \\ 0 & \kappa EI_{yz} & \kappa GJ_s + \kappa EI_y & GJ_s \end{bmatrix}, \tag{12c}$$

$$\widehat{\mathbf{P}}_3 = \begin{bmatrix} d\left(EA\right)^{(1)} & -d\kappa EA & 0 & 0 \\ d\kappa EA - 2\left(\kappa^{(1)}EI_z\right)^{(1)} & -2\left(\kappa^2 EI_z\right)^{(1)} & 0 & 2\left(\kappa EI_{yz}\right)^{(1)} \\ -2\left(\kappa^{(1)}EI_{yz}\right)^{(1)} & -2\left(\kappa^2 EI_{yz}\right)^{(1)} & \left(\kappa^2 GJ_s\right)^{(1)} & \left(\kappa GJ_s\right)^{(1)} + 2\left(\kappa EI_y\right)^{(1)} \\ 0 & 0 & \left(\kappa GJ_s\right)^{(1)} & \left(GJ_s\right)^{(1)} \end{bmatrix}, \tag{12d}$$

$$\widehat{\mathbf{P}}_4 = \begin{bmatrix} -\left(\kappa^{(1)}\right)^2 EI_z & -d\left(\kappa EA\right)^{(1)} - \kappa^{(1)}\kappa^2 EI_z & 0 & \kappa^{(1)}\kappa EI_{yz} \\ -\left(\kappa^{(1)}EI_z\right)^{(2)} - \kappa^{(1)}\kappa^2 EI_z & -d\kappa^2 EA - \left(\kappa^2 EI_z\right)^{(2)} - \kappa^4 EI_z & 0 & \left(\kappa EI_{yz}\right)^{(2)} + \kappa^3 EI_{yz} \\ -\left(\kappa^{(1)}EI_{yz}\right)^{(2)} & -\left(\kappa^2 EI_{yz}\right)^{(2)} & 0 & \left(\kappa EI_y\right)^{(2)} \\ \kappa^{(1)}\kappa EI_{yz} & \kappa^3 EI_{yz} & 0 & -\kappa^2 EI_y \end{bmatrix}, \tag{12e}$$

$$\widehat{\mathbf{R}}_4 = \begin{bmatrix} g\rho & 0 & 0 & 0 \\ 0 & g\rho & 0 & 0 \\ 0 & 0 & g\rho & 0 \\ 0 & 0 & 0 & gJ_s^m \end{bmatrix}, \tag{12f}$$

$$\widehat{\mathbf{P}} = -f \begin{bmatrix} p_x + \kappa m_z \\ p_y + \left(m_z\right)^{(1)} \\ q_z + \left(m_y\right)^{(1)} \\ m_x \end{bmatrix}. \tag{13}$$

Having determined matrix functions $\mathbf{Q}_m$ and $\mathbf{S}_m$ ($\mathbf{S}_m$ is calculated similarly as $\mathbf{Q}_m$ by substituting functions $\widehat{\mathbf{R}}_m$ for functions $\widehat{\mathbf{P}}_m$ in formula (A.10)) from formula (A.10) and expanded them and functions (13) into Chebyshev series and substituted the calculated series coefficients into (A.9), one gets the infinite system of ordinary differential equations

$$\begin{aligned} &\sum_{l=0}^{\infty}{}' \begin{bmatrix} k_{11}(k,l) & k_{12}(k,l) & k_{13}(k,l) & k_{14}(k,l) \\ k_{21}(k,l) & k_{22}(k,l) & k_{23}(k,l) & k_{24}(k,l) \\ k_{31}(k,l) & k_{32}(k,l) & k_{33}(k,l) & k_{34}(k,l) \\ k_{41}(k,l) & k_{42}(k,l) & k_{43}(k,l) & k_{44}(k,l) \end{bmatrix} \begin{bmatrix} u_l \\ v_l \\ w_l \\ \vartheta_l \end{bmatrix} \\ &= \begin{bmatrix} P_1(k) \\ P_2(k) \\ P_3(k) \\ P_4(k) \end{bmatrix} \\ &+ \sum_{l=0}^{\infty}{}' \begin{bmatrix} b_{11}(k,l) & 0 & 0 & 0 \\ 0 & b_{22}(k,l) & 0 & 0 \\ 0 & 0 & b_{33}(k,l) & 0 \\ 0 & 0 & 0 & b_{44}(k,l) \end{bmatrix} \begin{bmatrix} \ddot{u}_l \\ \ddot{v}_l \\ \ddot{w}_l \\ \ddot{\vartheta}_l \end{bmatrix}, \\ &k = 0, 1, 2, 3, \ldots. \end{aligned} \tag{14}$$

At this stage of the solution the $k_{ij}(k,l)$, $i,j = 1,2,3,4$, elements in system of (14) are a linear combination of the coefficients of expansion of the "input functions" and the coefficients of expansion of their first and second derivatives. The term "input functions" applies to the products of the functions described in formula (B.4) (see Appendix B). After complex transformations involving the use of relation $a_l = (a_{l-1}^{(1)} - a_{l+1}^{(1)})/2l$, $l \neq 0$, where $a_l = a_l[f]$ and $a_l^{(p)} = a_l[\partial^p f/\partial x^p]$, coefficients $k_{ij}(k,l)$ become a linear combination of only the coefficients of expansion of the "input functions". A detailed description of the transformations can be found in the author's paper [29] in which the Euler beam vibration problem was analysed. The ultimate form of coefficients $k_{ij}(k,l)$, $b_{ii}(k,l)$, and $P_i(k)$ is presented in Appendix B.

The first blocks of (14) – $k = 0,1,2,3$ (i.e., sixteen equations) are satisfied identitywise (0=0). The equations are replaced with the twelve boundary conditions which have not been used so far. The number of the conditions follows from the order of the equations in system ((1a), (1b), (1c), and (1d)). In the formulation of the equations stemming from the boundary conditions at the arch's ends ($s = \mp 1$) one uses the expansions of displacement functions (6), formulas (2)-(7) for internal forces, and the following formulas for calculating the Chebyshev polynomials at points $s = \mp 1$

$$\begin{aligned} T_n^{(m)}(1) &= \begin{cases} 1 & \text{for } m = 0, \\ \dfrac{n}{(2m-1)!!} \displaystyle\prod_{k=-m+1}^{m-1} (n+k) & \text{for } m > 0, \end{cases} \\ T_n^{(m)}(-1) &= (-1)^{n-m} T_n^{(m)}(1). \end{aligned} \tag{15}$$

Exemplary equations for the two main ways of fixing the arch are expressed by the formulas:

(i) clamped end (respectively on the left and right end of the arch)

$$\begin{aligned} u(-1,t) &= \sum_{l=0}^{\infty}{}' (-1)^l u_l = 0, & u(1,t) &= \sum_{l=0}^{\infty}{}' u_l = 0, \\ v(-1,t) &= \sum_{l=0}^{\infty}{}' (-1)^l v_l = 0, & v(1,t) &= \sum_{l=0}^{\infty}{}' v_l = 0, \\ \vartheta(-1,t) &= \sum_{l=0}^{\infty}{}' (-1)^l \vartheta_l = 0, & \vartheta(1,t) &= \sum_{l=0}^{\infty}{}' \vartheta_l = 0, \\ w(-1,t) &= \sum_{l=0}^{\infty}{}' (-1)^l w_l = 0, & w(1,t) &= \sum_{l=0}^{\infty}{}' w_l = 0, \\ \frac{\partial v(-1,t)}{\partial s} + \kappa u(-1,t) &= -\sum_{l=0}^{\infty}{}' (-1)^l l^2 v_l = 0, & \frac{\partial v(1,t)}{\partial s} + \kappa u(1,t) &= \sum_{l=0}^{\infty}{}' l^2 v_l = 0, \\ \frac{\partial w(-1,t)}{\partial s} &= -\sum_{l=0}^{\infty}{}' (-1)^l l^2 w_l = 0, & \frac{\partial w(1,t)}{\partial s} &= \sum_{l=0}^{\infty}{}' l^2 w_l = 0, \end{aligned} \tag{16}$$

(ii) hinged end
the first five equations are identical as $(16)_{1,2,3,4,6}$, whereas the sixth equation stems from the condition $m(-1,t)=0, m(1,t)=0$ and has the form

$$\frac{\partial^2 v(-1,t)}{\partial s^2} = \frac{1}{3}\sum_{l=0}^{\infty}{}' (-1)^l l^2 \left(l^2-1\right) v_l = 0,$$
$$\frac{\partial^2 v(1,t)}{\partial s^2} = \frac{1}{3}\sum_{l=0}^{\infty}{}' l^2 \left(l^2-1\right) v_l = 0. \tag{17}$$

In order to solve the modified system of (14) it was reduced to the finite system of equations $N = 4(m+1)$. This is tantamount to the assumption that each of the displacement functions in formula (10) is approximated by a finite series with $m+1$ terms. When the order of the terms is changed, the system is expressed by the formula

$$\mathbf{K}\mathbf{q}(t) + g\mathbf{B}\ddot{\mathbf{q}}(t) = \mathbf{F}(t), \tag{18}$$

where $\mathbf{q}(t) = \left[\mathbf{u}(t)\ \ \mathbf{v}(t)\ \ \mathbf{w}(t)\ \ \boldsymbol{\theta}(t)\right]^{\mathrm{T}}$, a $\mathbf{u} = [u_0, u_1, u_2, \ldots, u_m]^{\mathrm{T}}$, $\mathbf{v} = [v_0, v_1, v_2, \ldots, v_m]^{\mathrm{T}}$, $\mathbf{w} = [w_0, w_1, w_2, \ldots, w_m]^{\mathrm{T}}$, and $\boldsymbol{\theta} = [\vartheta_0, \vartheta_1, \vartheta_2, \ldots, \vartheta_m]^{\mathrm{T}}$.

System of (18) is further transformed. After left multiplying (18) by $\mathbf{K}^{-1}$ and using the theorem presented in Appendix C, matrix $\mathbf{K}^{-1}\mathbf{B}$ was reduced to the Jordan form. For the analysed system the solution of the eigenproblem

$$\left(g\mathbf{K}^{-1}\mathbf{B} - \lambda\mathbf{I}\right)\mathbf{q} = \mathbf{0} \tag{19}$$

leads to single eigenvalues λ, the transformation matrix has the form $\mathbf{S} = \mathbf{W}^{-1}$, where $\mathbf{W}$ is an eigenmatrix obtained by solving eigenproblem (19), and the matrix $\mathbf{J} = \{\lambda\} = \mathrm{diag}[\lambda_1, \lambda_2, \ldots, \lambda_n]$ becomes a diagonal matrix.

After substituting $\mathbf{q}(t) = \mathbf{S}^{-1}\mathbf{r}(t) = \mathbf{W}\mathbf{r}(t)$, introducing nondimensional time $\tau = t/\sqrt{g} = t\sqrt{EI_0/a^4\rho_0}$, adding a component describing the dumping, and making some simple transformations, system (18) was reduced to the system of separated equations

$$\{\lambda\}\ddot{\mathbf{r}}(\tau) + \left\{2\alpha\sqrt{\lambda}\right\}\dot{\mathbf{r}}(\tau) + \mathbf{r}(\tau) = \mathbf{W}^{-1}\mathbf{K}^{-1}\mathbf{F} = \mathbf{f}(\tau) \tag{20}$$

In order to reduce the computing time and eliminate the vibration forms encumbered with a large error (the eigenforms corresponding to the higher complex vibrational frequencies), the incorrect (inessential) eigenforms should be rejected. In this case, $k < N$ eigenforms are considered and transformation matrices $\mathbf{W}$ and $\mathbf{W}^{-1}$ then become rectangular matrices with, respectively, $N \times k$ and $k \times N$ dimensions (Kleiber et al. [33], p.128), and vector $\mathbf{r} = [r_1, r_2, \ldots, r_k]^{\mathrm{T}}$.

The $h_j(\tau)$ solution of the single equation from system of separated equations (20), when the function describing the load has the form $f_j(\tau) = 1\delta(\tau)$ (the Green function), is described by the formula

$$h_j(\tau) = \frac{\omega_j}{\sqrt{1-\alpha_j^2}} \exp\left(-\alpha_j\omega_j\tau\right)\sin\omega_j'\tau, \tag{21}$$

where $\omega_j = 1/\sqrt{\lambda_j}$, $\omega_j' = \omega_j\sqrt{1-\alpha_j^2}$. In the case of the load described by any function, the solution was obtained by calculating the convolution of the load and the Green function.

$$r_j(\tau) = \frac{\omega_j}{\sqrt{1-\alpha_j^2}} \cdot \int_0^{\tau} f_j(s)\exp\left(-\alpha_j\omega_j(\tau-s)\right)\sin\omega_j'(\tau-s)\,ds. \tag{22}$$

After all the components of vector $\mathbf{r}(t)$ had been calculated, the sought vector $\mathbf{q}(t) = \left[\mathbf{u}(t)\ \ \mathbf{v}(t)\ \ \mathbf{w}(t)\ \ \boldsymbol{\theta}(t)\right]^{\mathrm{T}} = \mathbf{W}\mathbf{r}(t)$ was determined.

4. Numerical Examples

In order to check the correctness and effectiveness of the proposed algorithm two examples are considered. In the first of the examples, systems taken from other authors' papers are solved with an aim of comparing the results obtained by the proposed method with the ones obtained by other methods. Example 2 shows how the method can be used to solve a more complex system, i.e., one with an arbitrarily variable curvature and cross section, subjected to any aperiodic load. In the examples the parameter defining the size of the approximation base amounts to m=20. The computations were performed using the Wolfram *Mathematica*® 7 software [34].

Example 1. A circular arch with length $2a = R\pi/3$, where R is the radius and $\pi/3$ is the opening angle ($\varphi \in \langle -\pi/6, \pi/6\rangle$), and a constant square ($b/h = 1$) cross section was analysed.

In the case of in-plane vibrations, two variants of arch clamping, stiff clamping at both ends (C-C) and hinged fixing (H-H), are assumed. In the case of out-of-plane vibrations, stiff clamping at both ends (C-C) is considered. The determined natural frequencies are nondimensional and defined by the formula $\lambda = \omega R^2\sqrt{\rho/EI}$, where R is the arch curvature radius. The calculations were performed for different values of parameter $k^2 = I/AR^2 = (h/R)^2/12$, assuming $h/R = 0.01$ and $h/R = 0.1$. It is apparent from the definition of parameter k that it indirectly defines the ratio of the beam's flexural stiffness to its axial stiffness.

The following methods were used to solve the eigenproblem:

(i) the method presented in this paper,

(ii) the analytical method, a close solution was obtained using *Mathematica*® [34],

(iii) the finite element method, where 3D nonprismatic (tapered) beam elements with six degrees of freedom in each node were used (*Cosmos/M*),

	Analytical	Analytical[a]	This paper	Classic	FEM_{20}	FEM_{100}	FEM_{500}
ω_1	31.7849	31.9414	31.8006	31.7849	31.7868	31.8250	31.8265
ω_2	33.4824	33.3856	33.4959	33.4824	32.9924	32.9670	32.9663
ω_3	80.0006	79.9723	80.0067	80.0240	77.5473	77.5392	77.5398
ω_4	107.549	107.592	107.550	107.523	107.324	107.187	107.182
ω_5	143.444	-	143.447	C*	136.019	136.022	136.024
ω_6	208.494	-	208.494	C	202.019	201.568	201.553
ω_7	225.319	-	225.321	C	214.369	213.864	213.846
ω_8	311.376	-	311.376	C	285.610	285.251	285.244
ω_9	324.594	-	324.596	C	317.177	314.476	314.370
					375.847	375.273	375.266
ω_{10}	416.206	-	416.206	C	424.336	417.776	417.517
ω_{11}	440.240	-	440.242	C			
ω_{12}	520.547	-	520.547	C	520.547	521.585	521.078

[a] the results obtained by Chidamparam and Leissa [1]
* C denotes complex values

Figure 2: Nondimensional in-plane free vibration frequencies of H-H circular arch for $h/R = 0.1$.

(iv) the approximation method based on classic power polynomials (Taylor series), where the sought displacements and rotation angles are described by the formulas

$$f(s) = \sum_{k=0}^{\infty} f_k \frac{s^k}{k!},$$
$$f^{(p)}(s) = \sum_{k=0}^{\infty} f_{k+p} \frac{s^k}{k!}, \quad \text{where } f = u, v, w, \vartheta. \tag{23}$$

In the case of numerical approximation method calculations, each of the functions u, v, w, ϑ was approximated with 30 terms of the series, whereas for FEM the system was divided into 20 finite elements. Such a number of finite elements (20) were selected that the number of parameters in FEM and the number of parameters in the approximation methods were equal or almost equal. In the case of the approximation methods, 120 parameters were defined (four functions x 30 terms of the series), while in FEM there were 126 generalized coordinates (21 nodes x 6 coordinates) minus the coordinates eliminated from the calculations due to the assumed boundary conditions. The reason why "only" 20 elements were used was to compare the effectiveness of the two types of approximation (the approximation presented in this paper and the FEM approximation) as applied to the considered problem. In order to verify the convergence of the solutions obtained by FEM the calculations were also performed for a much denser finite element grid – by dividing the arch into respectively 100 and 500 finite elements. To ensure that the comparisons were made for the same systems the values of all the geometric characteristics defining the arch's cross section were directly input into the *Cosmos/M* program.

The results yielded by the approximate methods were compared with the exact analytical solution.

The first twelve eigenfrequencies were compared for each of the considered cases, where at the adopted approximation base numerical computations yielded complex values already for the third eigenfrequency or higher eigenfrequencies (depending on the case). The calculated frequencies (units rad/s) are shown in Figures 2, 3, 4, 5, 6, and 7.

The frequencies connected with "the same" eigenform are given in the same row in the tables. Some eigenforms determined using FEM are "transposed". For example, to the eigenform connected with eigenfrequency ω_{11} =440.240 rad/s (the analytical solution) corresponds frequency 375.266 rad/s in the FEM solution, which is frequency no. 10 in the latter. To the eigenform connected with eigenfrequency ω_{10}=416.206 rad/s (the analytical solution) corresponds frequency 417.517 rad/s in FEM, which is frequency no. 11 in the latter. In such cases, the frequencies corresponding to "the same" eigenform are connected with an arrow.

For comparison, also the natural frequencies obtained by other authors are included there. The results taken from Liu and Wu [1] (Figures 4 and 5) are for $k = 0$, i.e., for a model with neglected arch axial deformability.

In order to compare the eigenforms relative error functions were calculated from the formula

$$E(f) = \frac{\left| f(s) - \tilde{f}(s) \right|}{\left\| f(s) \right\|}, \tag{24}$$

where $f(s)$ is the close analytical solution, $\tilde{f}(s)$ is the approximate solution, and $\|f(s)\| = \sup_{-1 \le s \le 1} |f(s)|$.

The analytically determined eigenforms were normalized so that the maximum value of displacement $u, v(w, \vartheta)$ was equal to one. Considering that the eigenforms were determined with an accuracy to a constant multiplier, the other solutions were normalized so that the mean-square error was minimum

$$\int_{-1}^{1} \left(\tilde{f} - f \right)^2 ds = \min. \tag{25}$$

	Analytical	Analytical[a]	This paper	Classic	FEM_{20}	FEM_{100}	FEM_{500}
ω_1	34.6063	34.5822	34.6206	34.6063	34.4319	34.4209	34.4205
ω_2	53.1987	53.1327	53.2071	53.1986	52.3803	52.3641	52.3640
					105.584	105.542	105.541
ω_3	107.555	107.635	107.555	107.558	107.423	107.307	107.303
ω_4	109.362	109.226	109.366	109.517			
ω_5	181.545	-	181.548	191.282	170.980	170.887	170.886
ω_6	209.523	-	209.523	C	209.998	209.175	209.143
ω_7	271.446	-	271.448	C	248.267	248.056	248.054
ω_8	312.992	-	312.992	C	315.047	312.386	312.281
ω_9	379.196	-	379.197	C	335.618	335.096	335.088
ω_{10}	416.790	-	416.790	C	431.578	429.983	429.955
ω_{11}	504.874	-	504.875	C	528.555	519.909	519.452
ω_{12}	520.684	-	520.684	C	536.313	530.704	530.642

Figure 3: Nondimensional in-plane free vibration frequencies of C-C circular arch for $h/R = 0.1$.

	Analytical	Analytical[a]	Paper[b]	This paper	Classic	FEM_{20}	FEM_{100}	FEM_{500}
ω_1	33.6248	33.6239	33.6261	33.6385	33.6248	33.6430	33.6179	33.6173
ω_2	74.8447	74.8387	75.0806	74.8513	74.8449	74.9703	74.8026	74.7967
ω_3	141.568	141.565	-	141.572	C	141.601	141.481	141.478
ω_4	216.419	216.394	-	216.421	C	216.973	216.269	216.244
ω_5	321.501	-	-	321.503	C	321.485	321.072	321.065
ω_6	335.415	-	-	335.417	C	334.446	335.437	335.475
ω_7	444.467	-	-	444.469	C	443.232	443.641	443.680
ω_8	573.280	-	-	573.281	C	573.339	571.922	571.906
ω_9	728.210	-	-	728.208	C	727.905	726.001	726.005
ω_{10}	896.013	-	-	896.003	C	897.392	892.745	892.698
ω_{11}	1087.50	-	-	1087.89	C	1089.08	1082.61	1082.60
ω_{12}	1092.20	-	-	1092.20	C	1091.86	1092.12	1092.13

[b]the results obtained by Liu and Wu [1].

Figure 4: Nondimensional in-plane free vibration frequencies of H-H circular arch for $h/R = 0.01$.

	Analytical	Analytical[a]	Paper[b]	This paper	Classic	FEM_{20}	FEM_{100}	FEM_{500}
ω_1	53.7360	53.7354	53.7402	53.7447	53.7359	53.7424	53.7246	53.7245
ω_2	98.4277	98.4265	99.4584	98.4327	98.4306	98.3901	98.3522	98.3520
ω_3	179.316	179.314	-	179.319	187.677	179.280	179.193	179.192
ω_4	250.075	250.072	-	250.077	208.463	250.074	249.917	249.916
ω_5	339.223	-	-	339.224	225.068	339.358	339.197	339.193
ω_6	377.008	-	-	377.009	C	376.863	376.471	376.470
ω_7	510.234	-	-	510.235	C	510.053	509.263	509.260
ω_8	646.318	-	-	646.318	C	646.264	644.720	644.716
ω_9	811.869	-	-	811.869	C	812.168	809.319	809.312
ω_{10}	982.549	-	-	982.548	C	983.765	979.064	979.053
ω_{11}	1094.76	-	-	1094.75	C	1096.16	1094.47	1094.38
ω_{12}	1188.77	-	-	1188.86	C	1191.55	1183.25	1183.23

Figure 5: Nondimensional in-plane free vibration frequencies of C-C circular arch for $h/R = 0.01$.

	Analytical	This paper	Classic	FEM_{20}	FEM_{100}	FEM_{500}
ω_1	19.5225	19.5225	19.5225	19.3754	19.3702	19.3702
ω_2	54.8783	54.8783	54.8782	53.7133	53.6996	53.6997
				64.4598	64.3730	64.3698
ω_3	108.643	108.643	108.626	105.584	104.227	105.541
ω_4	122.585	122.585	122.585			
				122.203	121.678	121.658
ω_5	180.425	180.425	190.013	168.668	168.567	168.566
				182.313	180.647	180.582
ω_6	231.427	231.427	223.016			
				244.201	240.353	240.201
ω_7	270.174	270.174	231.172	244.497	244.130	244.120
				308.321	301.018	300.731
ω_8	343.212	343.212	C			
ω_9	377.845	377.845	C	328.614	326.780	326.698
ω_{10}	455.812	455.812	C			
				375.847	364.536	364.104
ω_{11}	503.361	503.361		415.283	405.064	404.553
ω_{12}	568.808	568.808	C			

Figure 6: Nondimensional out-of-plane free vibration frequencies of C-C circular arch for $h/R = 0.1$.

	Analytical	This paper	Classic	FEM_{20}	FEM_{100}	FEM_{500}
ω_1	19.5440	19.5440	19.5440	19.5483	19.5427	19.5427
ω_2	54.9564	54.9564	54.9562	54.9586	54.9432	54.9432
ω_3	108.821	108.821	108.803	108.809	108.774	108.774
ω_4	180.740	180.740	190.379	180.688	180.612	180.612
ω_5	270.689	270.689	223.127	270.573	270.403	270.403
ω_6	378.654	378.654	C	378.463	378.094	378.093
ω_7	504.627	504.627	C	504.398	503.630	503.629
				641.808	641.141	641.110
ω_8	648.607	648.607	C	648.464	646.955	646.953
ω_9	810.590	810.589	C	810.801	808.004	808.000
ω_{10}	990.575	990.572	C	991.616	986.706	986.698
ω_{11}	1188.56	1188.65	C	1191.20	1182.99	1182.97
ω_{12}	1224.41	1224.41	C			

Figure 7: Nondimensional out-of-plane free vibration frequencies of C-C circular arch for $h/R = 0.01$.

Graphs of relative error functions (24) on the logarithmic scale, for selected eigenforms 1, 4, 8, and 12, are shown in Figures 8–10.

The relative error (relative to the exact analytical solution) of the first 12 eigenfrequencies determined using the proposed method is below $4.9 \cdot 10^{-4}$ for arch in-plane vibrations and below $7.4 \cdot 10^{-5}$ for arch out-of-plane vibrations. Although the classic series approximation yielded slightly more accurate results (the relative error of $2 \cdot 10^{-6}$) for the first two eigenfrequencies, the next eigenfrequencies are encumbered with an increasingly larger error (ranging from $1.4 \cdot 10^{-3}$ to $5.4 \cdot 10^{-2}$ in the case of arch $h/R = 0.01$ and from $4.7 \cdot 10^{-2}$ to $3.3 \cdot 10^{-1}$ in the case of arch $h/R = 0.1$), whereas the complex numbers obtained for eigenfrequencies 3-5 in the case of the hinge-supported arch and for eigenfrequencies 6-8 in the case of the stiff clamping were incommensurable. In the analysed interval of eigenfrequencies FEM yields results whose accuracy ranges from $5.0 \cdot 10^{-5}$ to $9.7 \cdot 10^{-2}$ for the H-H arch and from $1.2 \cdot 10^{-4}$ to $1.4 \cdot 10^{-1}$ for the C-C arch in the case of the eigenfrequencies describing the arch in-plane vibrations and from $7.5 \cdot 10^{-3}$ to $1.7 \cdot 10^{-1}$ ($4.5 \cdot 10^{-1}$ in isolated cases) in the case of the eigenfrequencies describing the arch out-of-plane vibrations.

An analysis of the obtained eigenvalues (Figures 2, 3, 4, 5, 6, 7) and the graphs of the relative errors (Figures 8–10) shows that the results yielded by the proposed method are considerably more precise than the ones obtained using the other methods.

In the case of eigenfrequencies, the relative error is smaller by several orders of magnitude than the errors of the other solution methods. Only the power series method yielded similarly accurate results for the first eigenforms. No further eigenforms were analysed because of the complex eigenfrequency values corresponding to them.

For the considered cases also the relative errors of the eigenforms were analysed at $h/R = 0.1$. The differences

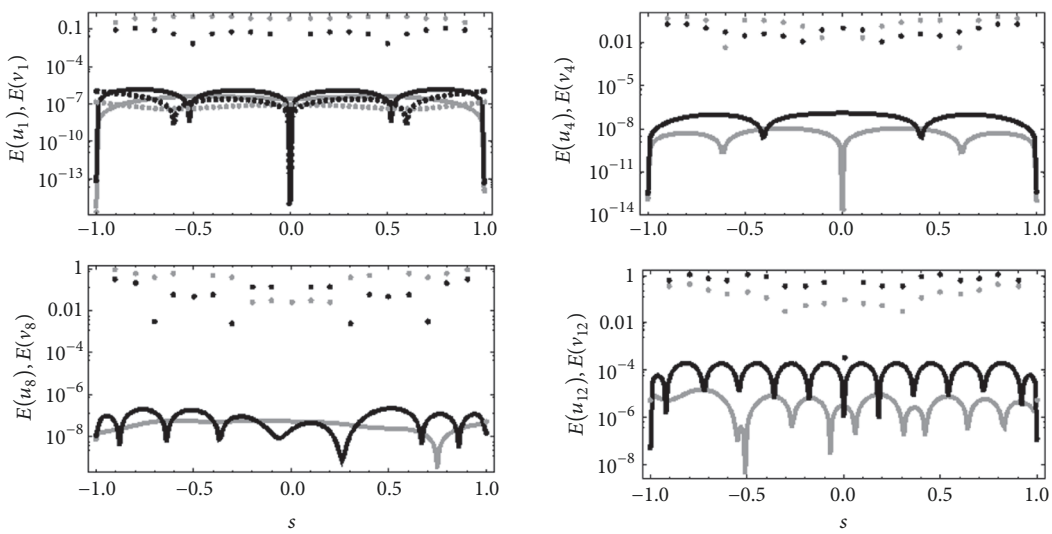

Figure 8: Graphs of relative errors $E(u_i)$ and $E(v_i)$ for selected eigenforms of H-H circular arch at $h/R = 0.01$ (in-plane vibrations). Denotations depending on method used to obtain solution: proposed method (—); FEM (• • • • •); classic series approximation (▪▪▪▪▪▪▪▪▪▪); black colour, u; grey colour, v.

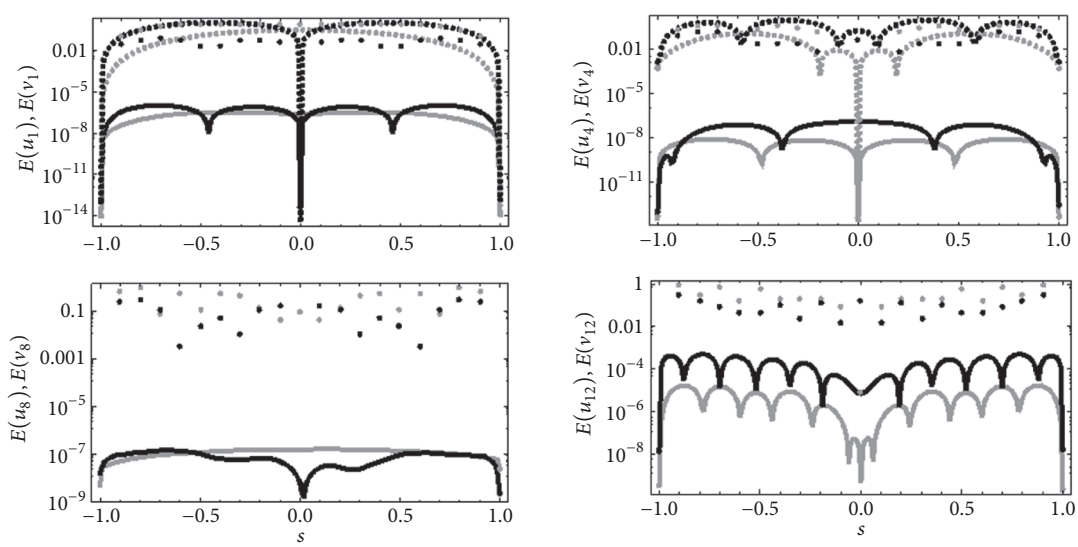

Figure 9: Graphs of relative errors $E(u_i)$ and $E(v_i)$ for selected eigenforms of C-C circular arch at $h/R = 0.01$ (in-plane vibrations). Denotations, depending on method used to obtain solution, as in Figure 8.

between the analytically determined eigenforms and the ones calculated using the proposed method for $h/R = 0.01$ were by 2-3 orders of magnitude smaller than the results discussed above for $h/R = 0.1$.

If one analyses the results presented in Figures 2, 3, 4, 5, 6, and 7, it becomes apparent that the "transposition" of the eigenforms in the case of the solutions obtained using FEM occurs mostly for out-of-plane vibration. Another observed regularity is the more frequent occurrence of "transpositions" for systems with $h/R = 0.1$ than for systems with $h/R = 0.01$ ("transpositions" occur more often in "stocky" systems). "Transpositions" are particularly numerous in Figure 6 (out-of-plane vibration and $h/R = 0.1$). All the "transpositions" occurring in Figures 6 and 7 concern "nearly pure" torsional modes, i.e., eigenforms in which the angle of cross section rotation ϑ is 2-3 orders higher than displacement w.

A comparison of the eigenfrequencies yielded by the proposed method (at the approximation base of 30 series terms) with the analytically determined eigenfrequencies shows that they are practically identical (in the adopted range of accuracy) or only slightly different.

Example 2. The algorithm is used here to solve the eigenproblem and the aperiodically forced vibration problem of a catenary nonprismatic arch. Two kinds of arch fixing: clamped-clamped (C-C) and hinged-hinged (H-H) are assumed. Static schemes of these arches are shown in Figures 11 and 12.

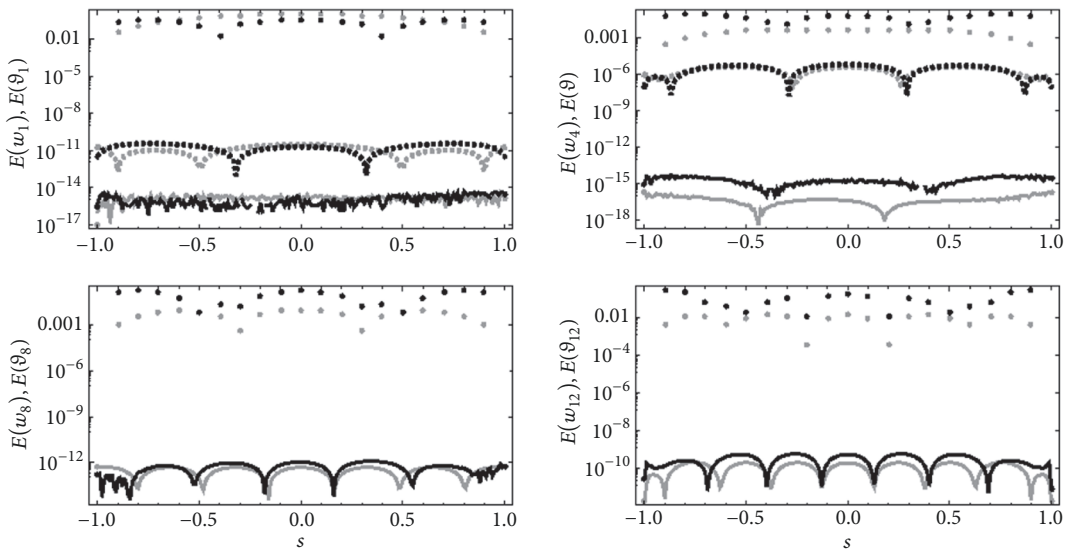

Figure 10: Graphs of relative errors $E(u_i)$ and $E(v_i)$ for selected eigenforms of C-C circular arch at $h/R = 0.01$ (out-of-plane vibrations). Denotations, depending on method used to obtain the solution, as in Figure 8.

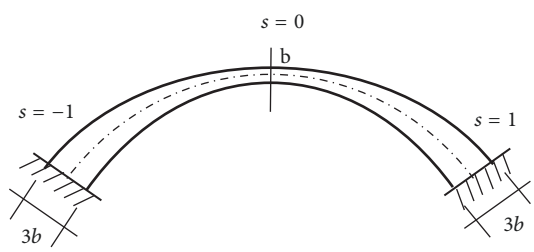

Figure 11: Clamped-clamped (C-C) arch system.

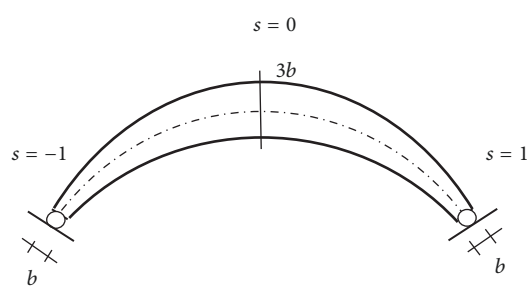

Figure 12: Hinged-hinged (H-H) arch system.

The parametric equations for the arch, as a function of its length, are as follows:

$$X = A \operatorname{arcsinh} \frac{S}{A},$$
$$Y = H + A - \sqrt{A^2 + S^2}, \tag{26}$$

where $H = A(\cosh L/A - 1)$ is the height and $2L$ is the span of the arch. Parameter A in formula (26) is a function of the assumed H/L ratio. The curvature of the arch is expressed by the formula

$$K(S) = \frac{A}{(A^2 + S^2)}. \tag{27}$$

$H/L = 3/4$ is assumed. Hence parameter A in formulas (26) and (27) is equal to 0.585874.

The cross section's height is described by the formulas

(i) for the clamped-clamped (C-C) arch

$$h(s) = b + x(s) = b + 2bs^2 \tag{28}$$

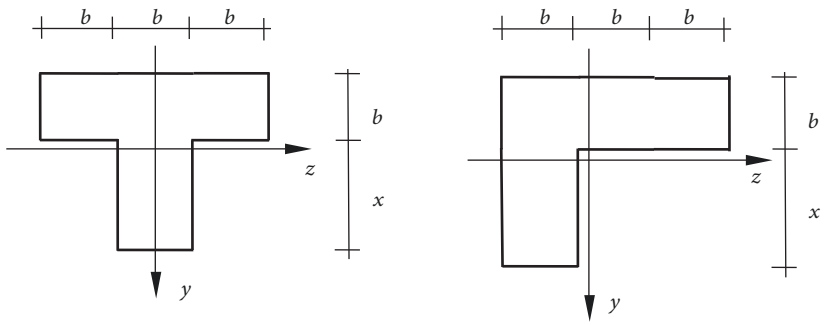

Figure 13: (a) Symmetric cross section (T). (b) Asymmetric cross section (L).

Table 1: Comparison of nondimensional natural frequencies for C-C arch.

	T cross section		L cross section	
	this paper	FEM	this paper	FEM
ω_1	12.8422	12.8357	14.4076	14.3977
ω_2	21.7808	21.5418	20.4538	20.2170
ω_3	35.456	35.3940	38.5603	38.4733
ω_4	43.0735	42.8782	41.0721	40.9014
ω_5	71.9845	71.6488	69.5107	69.2230
ω_6	73.4635	73.2456	77.2990	77.1129
ω_7	106.763	105.734	105.528	104.525
ω_8	125.614	124.971	125.176	124.907
ω_9	149.329	148.075	155.660	153.881
ω_{10}	181.214	188.195	171.785	174.332

Table 2: Comparison of nondimensional natural frequencies for H-H arch.

	T cross section		L cross section	
	this paper	FEM	this paper	FEM
ω_1	10.4339	10.4356	10.7314	10.7423
ω_2	16.1250	15.3052	15.3797	14.4755
ω_3	31.4425	31.4089	32.3181	32.3079
ω_4	41.4795	41.6023	38.7676	38.8465
ω_5	67.2877	67.1519	69.6218	69.5147
ω_6	77.8042	77.6857	73.0771	72.9532
ω_7	116.683	116.216	117.562	116.972
ω_8	122.193	121.738	118.982	118.508
ω_9	176.450	176.338	172.057	171.707
ω_{10}	177.627	177.575	176.415	175.082

(ii) for the hinged-hinged (H-H) arch

$$h(s) = b + x(s) = 3b - 2bs^2, \tag{29}$$

where $s = S/a$.

Two cross sections, a T cross section symmetric to the y axis and an asymmetric L cross section, were considered (see Figure 13) in each of the static schemes. Such shapes and dimensions of the cross sections were selected that the latter's areas and moments of inertia relative to the z axis were equal in both arch versions. The cross sections only differed in the moments of inertia relative to the y axis and in the moment of deviation (equal to zero for the T cross section and different from zero for the L cross section).

The eigenproblem was solved using the proposed method. Four cases, an arch with the symmetric T cross section and an arch with the asymmetric L cross section for each of the two arch clamping versions, were considered. Twenty terms of the series were used for approximation ($m = 19$). The same problem was solved using the FE method and forty finite elements with six degrees of freedom and a linearly variable cross section.

As a result of solving the eigenproblem, nondimensional natural frequencies $\omega = \Omega a^2 \sqrt{\rho_0/EI_0}$ were obtained, where $\rho_0 = \rho(0)$, $EI_0 = EI(0)$ for the C-C arch and $\rho_0 = \rho(-1) = \rho(1)$, $EI_0 = EI(-1) = EI(1)$ for the H-H arch. The first ten eigenfrequencies are presented in Tables 1 and 2.

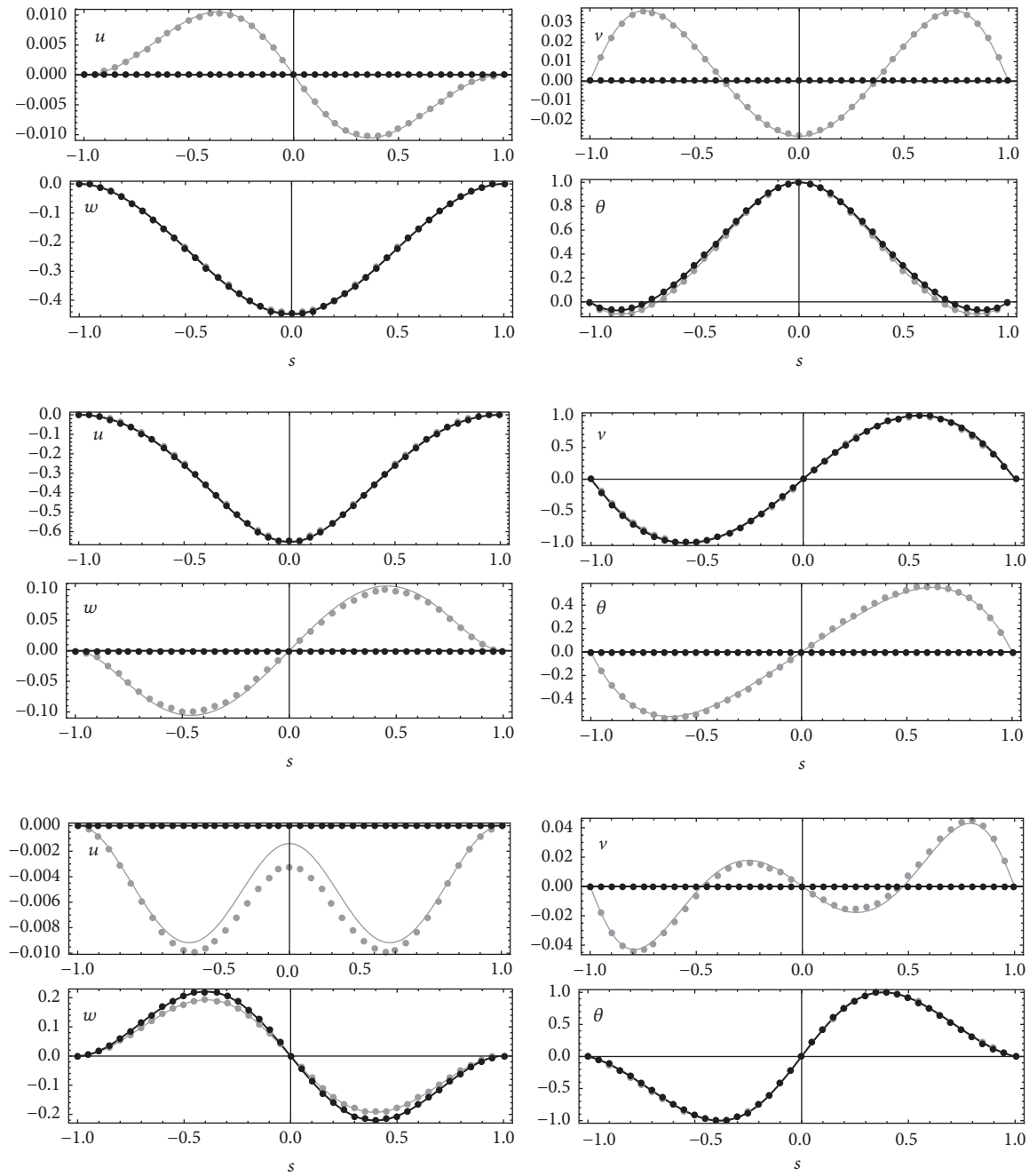

Figure 14: Graphs of H-H arch displacements u, v, w, ϑ for eigenforms nos. 1, 2, and 3, obtained using proposed method (—) and FEM (•••••); black colour, cross section T and grey colour, cross section L.

A comparison of the results obtained in this example shows high agreement between the natural frequencies calculated by the proposed method and the values yielded by FEM. In the case of the C-C arch, the maximum relative error between FEM and the proposed method for the first ten natural frequencies amounts to 3.709% and 1.461% for the T cross section and the L cross section, respectively. In the case of the H-H arch with the L cross section, the relative errors do not exceed 0.761%, except for the ω_2 frequency, for which the error amounts to 6.246%. Slightly better results were obtained in the case of the H-H arch with the T cross section, where as regards the first ten frequencies the maximum difference between the FEM results and the results yielded by the proposed method amounted to 0.402%, except for the ω_2 frequency, for which the relative error was 5.356%.

The first ten eigenforms were also compared for each of the arch clamping versions. The eigenforms nos. 1, 2, and 3 obtained by, respectively, the proposed method and the FE method are shown in Figures 14 and 15 (others eigenforms are not presented here due to the confines of this paper).

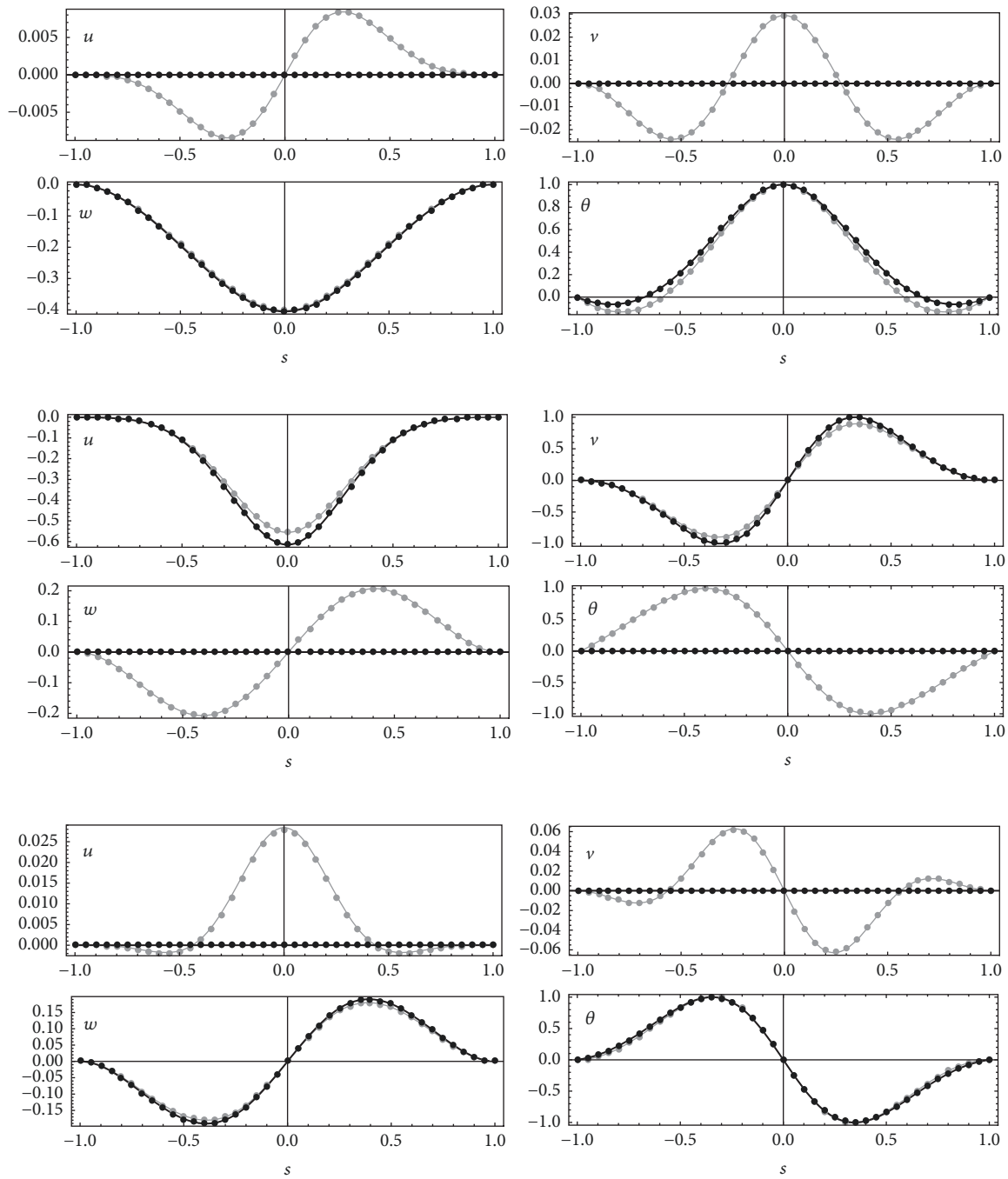

Figure 15: Graphs of C-C arch displacements u, v, w, ϑ for eigenforms nos. 1, 2, and 3, denotations as in Figure 14.

Figures 14 and 15 show good agreement between the eigenforms determined using the proposed method and the ones yielded by FEM. Up to eigenform 7 for the stiff clamping and up to eigenform 8 for the hinged fixing the graphs are practically identical. Single divergences appear at higher eigenforms (the latter are not presented here due to the confines of this paper).

By comparing the eigenfrequencies obtained for the systems with symmetric cross section T and asymmetric cross section L, the maximum differences between the eigenfrequencies were determined. The differences amount to 12.2% and 6.5% for, respectively, the C-C system and the H-H system.

In order to verify the convergence of the method the eigenproblem was solved for different approximation base sizes, i.e., $m + 1 = 10, 20, 30, 40, 50$ (formula (18)). The obtained results are shown in Tables 3 and 4.

Tables 3 and 4 show that the frequencies determined by the proposed method are convergent. It is also apparent that in the considered problems (20)-(30) terms of the series

Table 3: Nondimensional free vibration frequencies of H-H catenary arch (L cross section) for different approximation base sizes.

	ω_1	ω_2	ω_3	ω_4	ω_5	ω_6
m=10	10.6144	16.0092	32.0385	41.3351	72.7893	78.4554
m=20	10.7314	15.3797	32.3181	38.7676	69.6218	73.0771
m=30	10.7319	15.3489	32.3171	38.8423	69.6606	73.1144
m=40	10.7319	15.3495	32.3171	38.8412	69.6606	73.1136
m=50	10.7319	15.3495	32.3171	38.8412	69.6606	73.1136

Table 4: Nondimensional free vibration frequencies of H-H catenary arch (T cross section) for different approximation base sizes.

	ω_1	ω_2	ω_3	ω_4	ω_5	ω_6
m=10	10.1918	17.0051	30.8936	46.0632	72.2621	80.5428
m=20	10.4339	16.1250	31.4425	41.4795	67.2877	77.8042
m=30	10.4325	16.1013	31.4395	41.5974	67.3048	77.8800
m=40	10.4325	16.1019	31.4395	41.5959	67.3047	77.8794
m=50	10.4325	16.1019	31.4395	41.5959	67.3047	77.8794

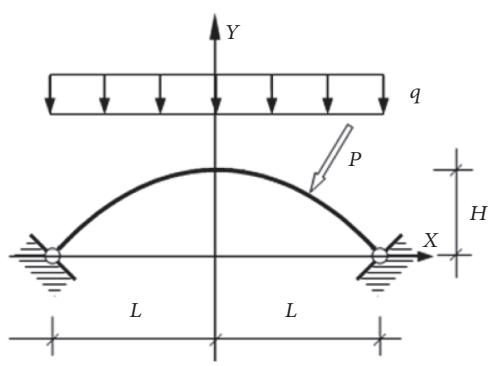

Figure 16: Analysed loading configurations.

need to be used for the approximation in order to obtain sufficiently accurate results.

As regards the aperiodically forced vibration problem, the vibrations of the hinged-hinged arch loaded in the plane of its axis were analysed. The problem was solved for two cases differing in the spatial distribution of the load. In the first case, the load with intensity $Q(S) = q$ was uniformly distributed as shown in Figure 16. In the second case the arch was loaded with concentrated force $Q(S) = P\delta(S - S_0)$, where $S_0 = 0.5a$, perpendicular to the arch (Figure 16). The force values were $q = 1000\,\mathrm{N/m}$, $P = 1000\,\mathrm{N}$. Calculations were performed assuming the following arch geometry parameters: b=0.01 m (Figure 13), $H/L = 3/4$ (Figure 16). The parameters of the material properties were $E = 205.0 \times 10^9\,\mathrm{N/m^2}$, $\rho_V = 7860\,\mathrm{kg/m^3}$, and $\alpha_j = \alpha = 0.015$.

Also two different cases of the time distribution of the load were considered. In the first case, the time distribution of the load had the form of a rectangular pulse and the load defining functions are expressed by

$$P(X,t) = Q(S)\left(\mathrm{H}(t) - \mathrm{H}(t-\Delta)\right), \tag{30}$$

where $\mathrm{H}(t)$ is the Heaviside function and $\Delta = 0.04\,\mathrm{s}$ is the pulse duration. In the second case, the time distribution had the form of the harmonic function

$$P(X,t) = Q(S)\,\mathrm{H}(t)\sin pt \tag{31}$$

The following functions of harmonic excitation p were assumed:

$$\begin{aligned} p_1 &= \omega_1^L = 158.346\ \mathrm{rad/s}, \\ p_2 &= \omega_1^T = 153.910\ \mathrm{rad/s}, \\ p_3 &= \frac{\left(\omega_1^L + \omega_1^T\right)}{2} = 156.128\ \mathrm{rad/s} \end{aligned} \tag{32}$$

where ω_1^L is the first natural frequency of the arch with the L cross section; ω_1^T is the first natural frequency of the arch with the T cross section. The out-of-plane vibrations correspond with frequency ω_1^T, whereas the coupled spatial vibrations, where displacements w and cross section rotation ϑ are one order of magnitude higher than displacements u, v, correspond with frequency ω_1^L.

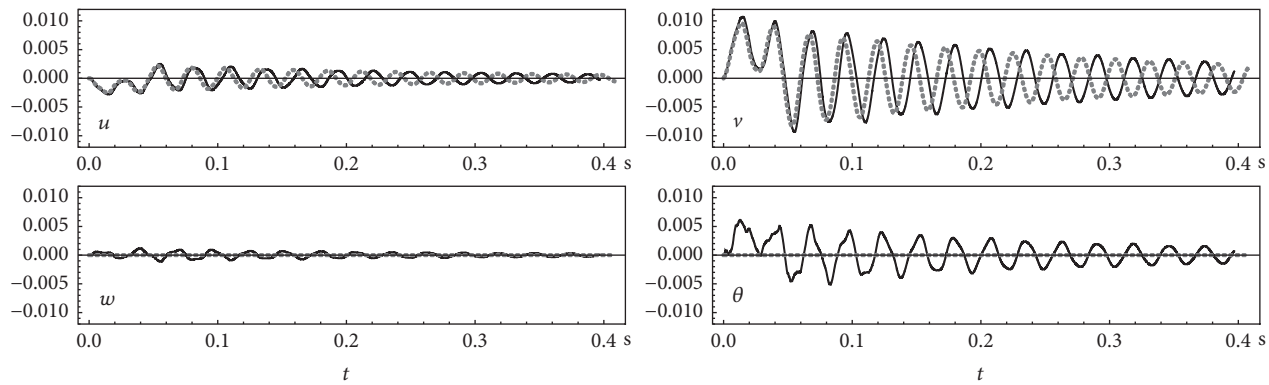

Figure 17: Graphs of displacements $u(0.5,t)$, $v(0.5,t)$, $w(0.5,t)$, $\vartheta(0.5,t)$ induced by load $P(X,t) = P\delta(S-0.5a)\ (\mathrm{H}(t)-\mathrm{H}(t-\Delta))$. Denotations: the black continuous line represents the solution for the arch with asymmetric cross section L while the grey dotted line denotes the solution for the arch with symmetric cross section T.

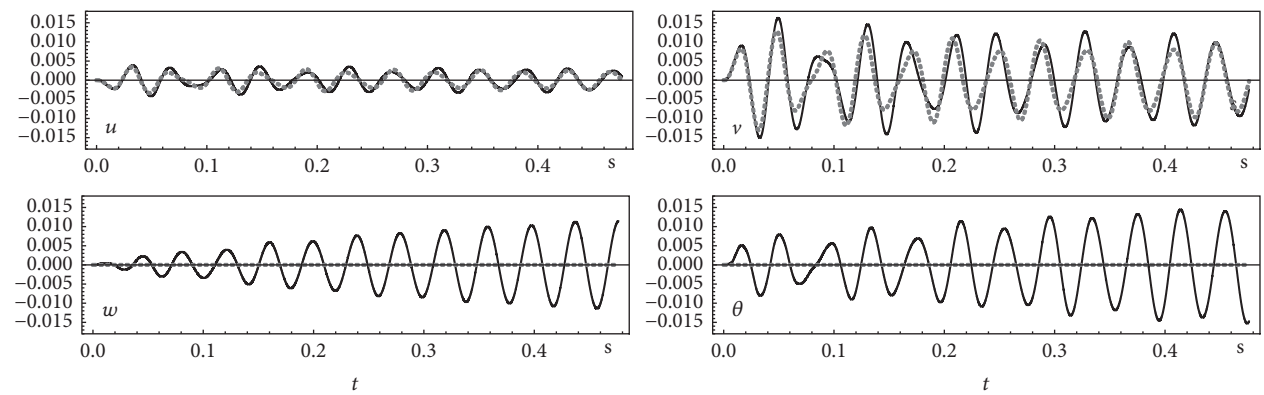

Figure 18: Graphs of displacements $u(0.5,t)$, $v(0.5,t)$, $w(0.5,t)$, $\vartheta(0.5,t)$ induced by load $P(X,t) = P\delta(S-0.5a)\ \mathrm{H}(t)\sin p_1 t)$. Denotations as in Figure 17.

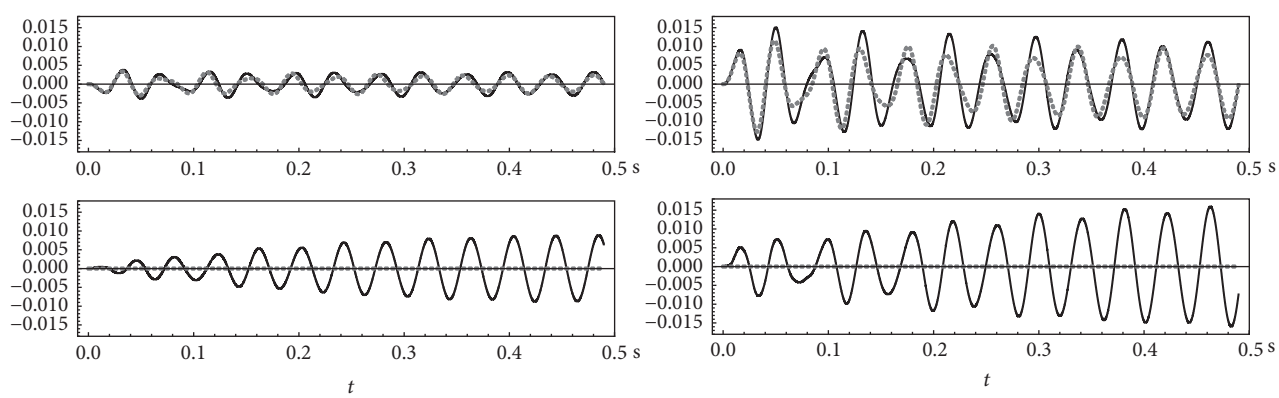

Figure 19: Graphs of displacements $u(0.5,t)$, $v(0.5,t)$, $w(0.5,t)$, $\vartheta(0.5,t)$ induced by load $P(X,t) = P\delta(S-0.5a)\ \mathrm{H}(t)\sin p_2 t)$. Denotations as in Figure 17.

The results in the form of the displacement functions $u(0.5,t)$, $v(0.5,t)$, $w(0.5,t)$ and rotation function $\vartheta(0.5,t)$ for point $s = 0.5$ are shown in Figures 17–24.

An analysis of the above results shows that when the system is loaded with a concentrated force, the system's responses (the three displacements and the rotation) in the investigated point are of the same order of magnitude. The exception are the vibrations induced by load pulses, where displacements w are by one order of magnitude smaller than displacements v. Moreover, in the case of the nonstationary vibrations induced by the harmonic load, displacements u are several times smaller than displacements v and w. In

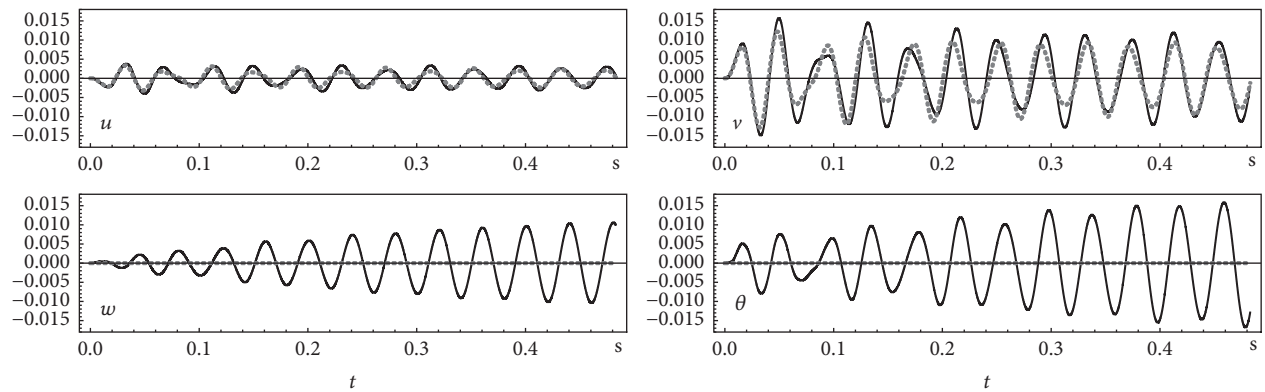

Figure 20: Graphs of displacements $u(0.5, t)$, $v(0.5, t)$, $w(0.5, t)$, $\vartheta(0.5, t)$ induced by load $P(X, t) = P\delta(S - 0.5a)\ \mathrm{H}(t)\ \sin p_3 t)$. Denotations as in Figure 17.

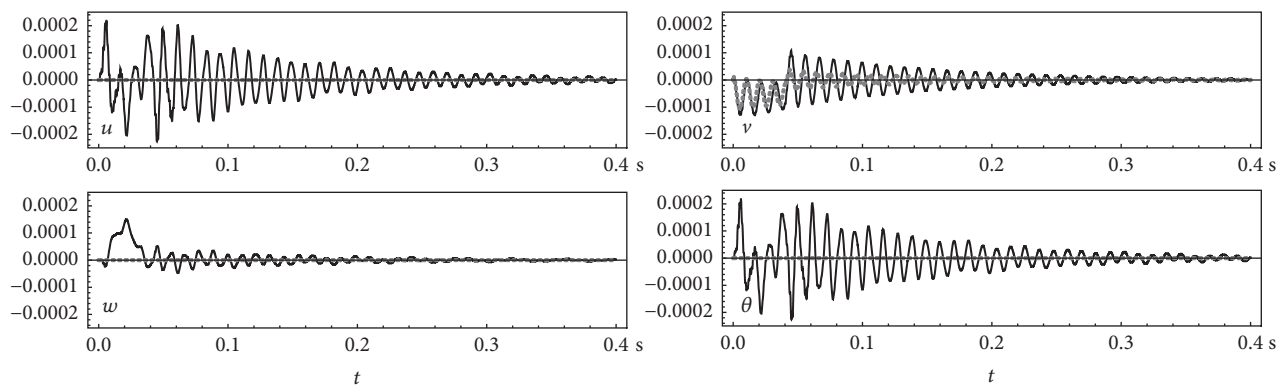

Figure 21: Graphs of displacements $u(0.5, t)$, $v(0.5, t)$, $w(0.5, t)$, $\vartheta(0.5, t)$ induced by load $P(X, t) = q\ \ (\mathrm{H}(t) - \mathrm{H}(t - \Delta))$. Denotations as in Figure 17.

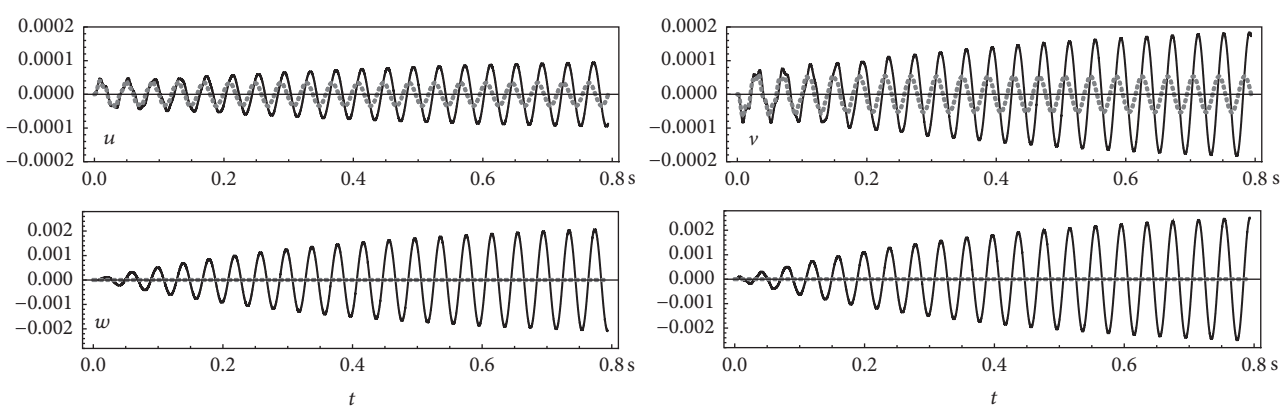

Figure 22: Graphs of displacements $u(0.5, t)$, $v(0.5, t)$, $w(0.5, t)$, $\vartheta(0.5, t)$ induced by load $P(X, t) = q\ \mathrm{H}(t) \sin p_1 t)$. Denotations as in Figure 17.

the case of the vibrations induced by the load applied at a constant rate, all the displacements and the rotation are of the same order of magnitude, irrespective of the type of excitation (pulse or harmonic). In the case of the nonstationary vibrations of the L system, induced by the harmonic load, vibration amplifications (increases in vibration over time) are visible. Besides displacements u, v, also displacement w and rotation ϑ are amplified, despite the fact that the load acts in the plane of the arch. The occurrence of displacements characteristic of out-of-plane arch vibrations is due to the appearance of conjugating elements $k_{ij}(k, l)$, $k_{ji}(k, l)$, where $i = 1, 2$; $j = 3, 4$, in system of (14). The amplification of the values of functions w and ϑ is due to the amplification of vibrations in the resonance zone since excitation frequency

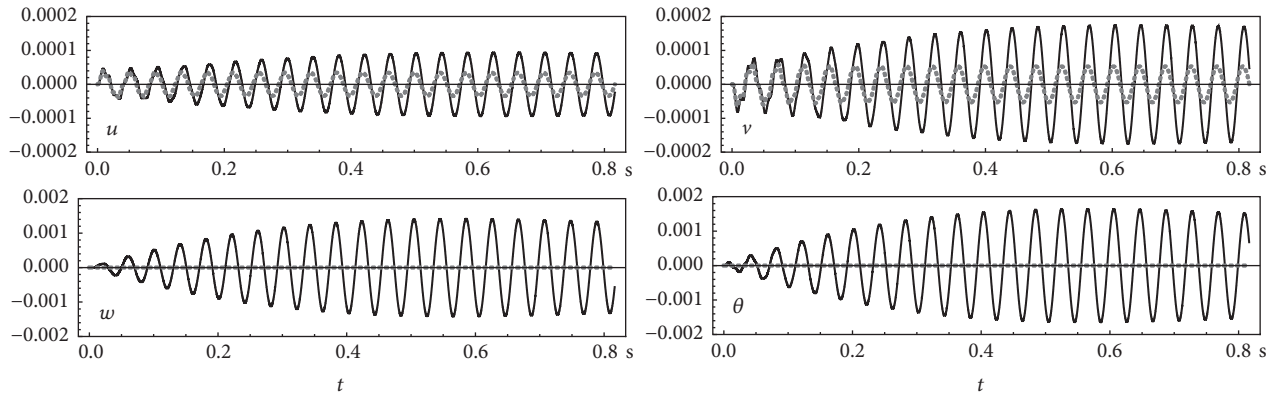

Figure 23: Graphs of displacements $u(0.5, t)$, $v(0.5, t)$, $w(0.5, t)$, $\vartheta(0.5, t)$ induced by load $P(X, t) = q\,\mathrm{H}(t) \sin p_2 t)$. Denotations as in Figure 17.

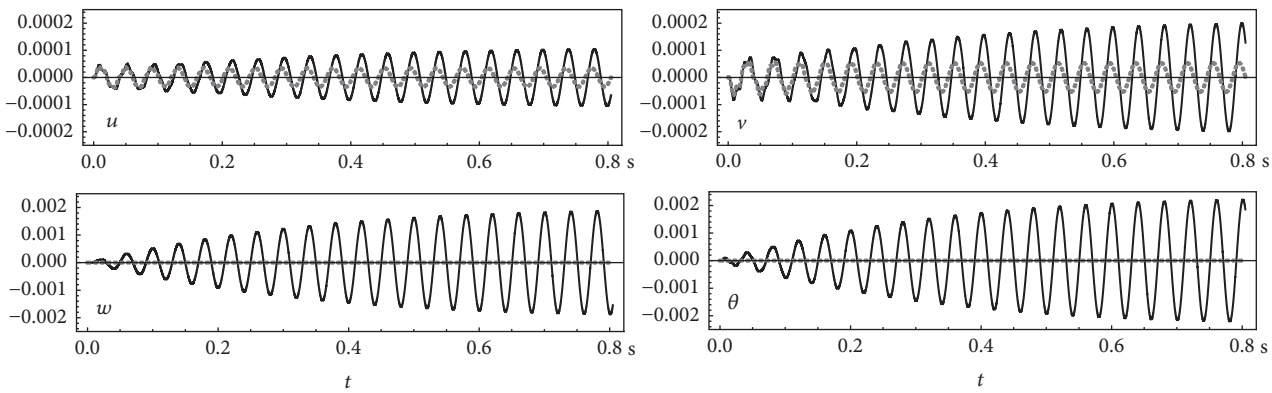

Figure 24: Graphs of displacements $u(0.5, t)$, $v(0.5, t)$, $w(0.5, t)$, $\vartheta(0.5, t)$ induced by load $P(X, t) = q\,\mathrm{H}(t) \sin p_3 t)$. Denotations as in Figure 17.

ω_1^L is the eigenfrequency of the out-of-plane arch vibrations. Because of the separation of the equations describing the arch in-plane and out-of-plane vibrations ($k_{ij}(k, l) = 0$, $k_{ji}(k, l) = 0$, where $i = 1, 2$; $j = 3, 4$) and the direction of the load (in the plane of the arch), no displacements characteristic of arch out-of-plane vibrations appears: $w(0.5, t) = 0$, $\vartheta(0.5, t) = 0$.

5. Conclusion

The following general conclusions emerge from an analysis of the results obtained in the examples:

(i) The derived final equations (enabling one to directly calculate the coefficients of expansion of the sought functions) have a general character stemming from the analytical form of the coefficients of the equations. Owing to this the vibration problem can be solved for any arch, described in accordance with the Bernoulli-Euler theory, without it being necessary to derive the equations again.

(ii) The results obtained using the solution method proposed in this paper agree with the results obtained by other authors.

(iii) The comparison of the results obtained by the different methods (FEM, the approximation method based on the classic power series, and the proposed method) with the analytical results has shown that results yielded by the proposed method are much more accurate than the ones obtained by the other methods.

(iv) The method is highly accurate: already 30-power series element approximation yields results agreeing with the analytical solution results.

(v) The examples show that the proposed method is fast convergent (Tables 3 and 4). When the size of the approximation base is increased to $m = 30$, 40, and 50, the accuracy of the results increases only slightly in comparison with the accuracy of the results obtained when $m = 20$.

The following detailed conclusions can be drawn from the analysis of the effect of cross section asymmetry on the form the spatial vibrations of the arch:

(i) In the case of asymmetric cross sections, coupled vibrations are generated (arch in-plane vibrations are accompanied by out-of-plane vibrations and vice

versa). When displacements connected with out-of-plane vibrations dominate, the accompanying coupled in-plane vibrations are relatively small. Whereas when displacements connected with in-plane vibrations dominate, the coupled out-of-plane vibrations arising in the system are of the same order of magnitude as the dominant vibrations. This regularity is observed in the case of free vibrations (Figures 14 and 15).

(ii) The coupling of vibrations also occurs in the case of forced vibrations, especially when the vibrations are forced by a harmonically variable load. In the examples, even though the harmonic load acts in the plane of the arch, the out-of-plane vibrations are of the same order of magnitude as the in-plane vibrations. Since the excitation frequencies assume the resonant value or values close to those of the resonant frequencies, the characteristic increment in vibrations over time is visible in the vibration diagram.

Appendix

A. Approximation Method of Solving Differential Equations with Variable Coefficients

In this paper, in order to solve the system of differential equations a generalization of the following theorem concerning ordinary differential equations ([32] p. 231) is used.

Theorem A.1. *If function f satisfies a linear equation with order $n > 0$*

$$\sum_{m=0}^{n} \widehat{P}_m(x) f^{(n-m)}(x) = \widehat{P}(x), \tag{A.1}$$

$$Q_m(x) = \sum_{j=0}^{m} (-1)^{m+j} \binom{n-j}{m-j} \widehat{P}_j^{(m-j)}(x), \quad m = 0, 1, \ldots, n \tag{A.2}$$

where $\binom{n}{m} = n!/m!(n-m)!$ and functions $(Q_0 f)^{(n)}, (Q_1 f)^{(n-1)}, \ldots, Q_n f$, $\widehat{P}$ have determinable coefficients of the Chebyshev series, then for each integer k the following identity holds:

$$\sum_{m=0}^{n} 2^{n-m} \sum_{j=0}^{m} b_{nmj}(k)\, a_{k-m+2j}\left[Q_m(x) f(x)\right] = \sum_{j=0}^{n} b_{nnj}(k)\, a_{k-n+2j}\left[\widehat{P}(x)\right], \tag{A.3}$$

where $b_{nmj}(k)$ are polynomials of integer k

$$b_{nmj}(k) = (-1)^j \binom{m}{j} (k-n)_{n-m+j} (k-m+2j) \cdot (k+j+1)_{n-j} \left(k^2 - n^2\right)^{-1}, \quad m = 0, 1, \ldots, n;\ j = 0, 1, \ldots, m. \tag{A.4}$$

$$(k)_n = \begin{cases} 1 & \text{for } n = 0, \\ k(k+1)(k+2)\ldots(k+n-1) & \text{for } n = 1, 2, 3, \ldots, \end{cases} \tag{A.5}$$

and $a_k[h]$ is the k-th coefficient of expansion of function $h(x)$ into a Chebyshev series relative to Chebyshev polynomials of the 1st kind (the proof of this theorem can be found in [32] pp. 231-234).

The generalization of the theorem consists in the transference of the differential equation approximate solution method (described by the theorem) onto systems of linear differential equations (see [32] p. 323). In such a case, system of N equations can be presented in this matrix form

$$\sum_{m=0}^{n} \widehat{\mathbf{P}}_{\mathbf{m}}(x)\, \mathbf{f}^{(\mathbf{n-m})}(x) = \widehat{\mathbf{P}}(x), \tag{A.6}$$

where coefficients $\widehat{\mathbf{P}}_{\mathbf{m}}(x)$ are square matrices of degree N and $\mathbf{f}(x)$ and $\widehat{\mathbf{P}}(x)$ are N-element vectors. The differentiation of the vector means the differentiation of each of its components. If vector function $\mathbf{f}(x)$ satisfies system of (A.6) and the theorem's assumptions hold good, then for each integer k the following identity is true:

$$\sum_{m=0}^{n} 2^{n-m} \sum_{j=0}^{m} b_{nmj}(k)\, a_{k-m+2j}\left[\mathbf{Q}_{\mathbf{m}}(x)\, \mathbf{f}(x)\right] = \sum_{j=0}^{n} b_{nnj}(k)\, a_{k-n+2j}\left[\widehat{\mathbf{P}}(x)\right] \tag{A.7}$$

Functions $\mathbf{Q}_{\mathbf{m}}(x)$ in the formula are matrix equivalents of the functions defined by formula (A.2)

$$\mathbf{Q}_{\mathbf{m}}(x) = \sum_{j=0}^{m} (-1)^{m+j} \binom{n-j}{m-j} \widehat{\mathbf{P}}_{\mathbf{j}}^{(\mathbf{m-j})}(x), \quad m = 0, 1, \ldots, n, \tag{A.8}$$

and $a_l[\mathbf{Q}_{\mathbf{m}}(x)\mathbf{f}(x)]$ stands for a vector whose elements are the l-th coefficients of the Chebyshev expansion of the components of vector $\mathbf{Q}_{\mathbf{m}}(x)\mathbf{f}(x)$.

In a special case, when system of (A.6) is a 4th-order ($n = 4$) system, the sought coefficients $a_l[\mathbf{f}]$ of the Chebyshev expansion of vector function $\mathbf{f}$ satisfy the following infinite system of algebraic equations:

$$
\begin{aligned}
&\sum_{l=0}^{\infty}{}' \left\{8\left(k^2-9\right)\left(k^2-4\right)\left(k^2-1\right)k\left(a_{k-l}\left[\mathbf{Q}_0\right]+a_{k+l}\left[\mathbf{Q}_0\right]\right)\right.\\
&+4\left(k^2-9\right)\left(k^2-4\right)\left(k^2-1\right)\left(a_{k-l-1}\left[\mathbf{Q}_1\right]+a_{k+l-1}\left[\mathbf{Q}_1\right]-a_{k-l+1}\left[\mathbf{Q}_1\right]-a_{k+l+1}\left[\mathbf{Q}_1\right]\right)\\
&+2\left(k^2-9\right)\left(k^2-4\right)\left((k+1)\left(a_{k-l-2}\left[\mathbf{Q}_2\right]+a_{k+l-2}\left[\mathbf{Q}_2\right]\right)-2k\left(a_{k-l}\left[\mathbf{Q}_2\right]+a_{k+l}\left[\mathbf{Q}_2\right]\right)\right.\\
&\left.+(k-1)\left(a_{k-l+2}\left[\mathbf{Q}_2\right]+a_{k+l+2}\left[\mathbf{Q}_2\right]\right)\right)\\
&+\left(k^2-9\right)\left((k+1)(k+2)\left(a_{k-l-3}\left[\mathbf{Q}_3\right]+a_{k+l-3}\left[\mathbf{Q}_3\right]\right)-3(k-1)(k+2)\left(a_{k-l-1}\left[\mathbf{Q}_3\right]+a_{k+l-1}\left[\mathbf{Q}_3\right]\right)\right.\\
&\left.+3(k+1)(k-2)\left(a_{k-l+1}\left[\mathbf{Q}_3\right]+a_{k+l+1}\left[\mathbf{Q}_3\right]\right)-(k-1)(k-2)\left(a_{k-l+3}\left[\mathbf{Q}_3\right]+a_{k+l+3}\left[\mathbf{Q}_3\right]\right)\right)\\
&+\frac{1}{2}\left((k+1)(k+2)(k+3)\left(a_{k-l-4}\left[\mathbf{Q}_4\right]+a_{k+l-4}\left[\mathbf{Q}_4\right]\right)-4(k+3)\left(k^2-4\right)\left(a_{k-l-2}\left[\mathbf{Q}_4\right]+a_{k+l-2}\left[\mathbf{Q}_4\right]\right)\right.\\
&+6k\left(k^2-9\right)\left(a_{k-l}\left[\mathbf{Q}_4\right]+a_{k+l}\left[\mathbf{Q}_4\right]\right)-4(k-3)\left(k^2-4\right)\left(a_{k-l+2}\left[\mathbf{Q}_4\right]+a_{k+l+2}\left[\mathbf{Q}_4\right]\right)\\
&\left.\left.+(k-1)(k-2)(k-3)\left(a_{k-l+4}\left[\mathbf{Q}_4\right]+a_{k+l+4}\left[\mathbf{Q}_4\right]\right)\right)\right\}a_l[f]\\
&=(k+1)(k+2)(k+3)a_{k-4}\left[\widehat{\mathbf{P}}\right]-4(k+3)\left(k^2-4\right)a_{k-2}\left[\widehat{\mathbf{P}}\right]+6k\left(k^2-9\right)a_k\left[\widehat{\mathbf{P}}\right]\\
&-4(k-3)\left(k^2-4\right)a_{k+2}\left[\widehat{\mathbf{P}}\right]+(k-1)(k-2)(k-3)a_{k+4}\left[\widehat{\mathbf{P}}\right],\\
&\qquad\qquad 0,1,2,3,\ldots
\end{aligned}
\tag{A.9}
$$

where

$$
\begin{aligned}
\mathbf{Q}_0&=\widehat{\mathbf{P}}_0,\\
\mathbf{Q}_1&=-4\widehat{\mathbf{P}}_0{}^{(1)}+\widehat{\mathbf{P}}_1,\\
\mathbf{Q}_2&=6\widehat{\mathbf{P}}_0{}^{(2)}-3\widehat{\mathbf{P}}_1{}^{(1)}+\widehat{\mathbf{P}}_2,\\
\mathbf{Q}_3&=-4\widehat{\mathbf{P}}_0{}^{(3)}+3\widehat{\mathbf{P}}_1{}^{(2)}-2\widehat{\mathbf{P}}_2{}^{(1)}+\widehat{\mathbf{P}}_3,\\
\mathbf{Q}_4&=\widehat{\mathbf{P}}_0{}^{(4)}-\widehat{\mathbf{P}}_1{}^{(3)}+\widehat{\mathbf{P}}_2{}^{(2)}-\widehat{\mathbf{P}}_3{}^{(1)}+\widehat{\mathbf{P}}_3,
\end{aligned}
\tag{A.10}
$$

The general form of the theorems can be found in the cited above work and in the author's papers [30, 31].

B. The Elements of Matrix Equation of Motion

The elements of matrix equation of motion (14) are expressed as follows:

$$
\begin{aligned}
k_{11}(k,l)=\;&2d\left(k^2-9\right)l\left((k+1)(k+2)\left(a_{k-l-2}-a_{k+l-2}\right)\right.\\
&\left.-2\left(k^2-4\right)\left(a_{k-l}-a_{k+l}\right)+(k-1)(k-2)\left(a_{k-l+2}-a_{k+l+2}\right)\right)\\
&-\frac{1}{2}\left((k+1)(k+2)(k+3)\left(\kappa_2^0 el_{k-l-4}+\kappa_2^0 el_{k+l-4}\right)\right.\\
&-4(k+3)\left(k^2-4\right)\left(\kappa_2^0 el_{k-l-2}+\kappa_2^0 el_{k+l-2}\right)\\
&+6k\left(k^2-9\right)\left(\kappa_2^0 el_{k-l}+\kappa_2^0 el_{k+l}\right)-4(k-3)\left(k^2-4\right)\left(\kappa_2^0 el_{k-l+2}+\kappa_2^0 el_{k+l+2}\right)\\
&\left.+(k-1)(k-2)(k-3)\left(\kappa_2^0 el_{k-l+4}+\kappa_2^0 el_{k+l+4}\right)\right)
\end{aligned}
\tag{B.1a}
$$

$$
\begin{aligned}
k_{12}(k,l)=\;&-2l\left[(k+1)(k+2)(k+3)\left((l-1)\kappa_1^0 el_{k-l-2}+(l+1)\kappa_1^0 el_{k+l-2}\right)\right.\\
&-2\left((k-2)(k-3)(6+(k+5)l)\kappa_1^0 el_{k-l}+(k+2)(k+3)(6-(k-5)l)\kappa_1^0 el_{k+l}\right)
\end{aligned}
$$

$$
\begin{aligned}
&+(k-1)(k-2)(k-3)\left((l-1)\kappa_1^0 el_{k-l+2}+(l+1)\kappa_1^0 el_{k+l+2}\right)\\
&-120\sum_{j=0}^{l}(k+2j-l)\kappa_1^0 el_{k+2j-l}\Bigg]\\
&-2d\left(k^2-9\right)\Big((k+1)(k+2)\left(\kappa^1 a_{k-l-3}+\kappa^1 a_{k+l-3}\right)-3(k-1)(k+2)\left(\kappa^1 a_{k-l-1}+\kappa^1 a_{k+l-1}\right)\\
&+3(k+1)(k-2)\left(\kappa^1 a_{k-l+1}+\kappa^1 a_{k+l+1}\right)+(k-1)(k-2)\left(\kappa^1 a_{k-l+3}+\kappa^1 a_{k+l+3}\right)\Big)\\
&-\frac{1}{2}\Big((k+1)(k+2)(k+3)\left(\kappa_1^2 el_{k-l-4}+\kappa_1^2 el_{k+l-4}\right)-4(k+3)\left(k^2-4\right)\left(\kappa_1^2 el_{k-l-2}+\kappa_1^2 el_{k+l-2}\right)\\
&+6k\left(k^2-9\right)\left(\kappa_1^2 el_{k-l}+\kappa_1^2 el_{k+l}\right)-4(k-3)\left(k^2-4\right)\left(\kappa_1^2 el_{k-l+2}+\kappa_1^2 el_{k+l+2}\right)\\
&+(k-1)(k-2)(k-3)\left(\kappa_1^2 el_{k-l+4}+\kappa_1^2 el_{k+l+4}\right)\Big)
\end{aligned}
\tag{B.1b}
$$

$$
\begin{aligned}
k_{13}(k,l)=&-2l\Bigg[(k+1)(k+2)(k+3)\left((l-1)\kappa_1^0 es_{k-l-2}+(l+1)\kappa_1^0 es_{k+l-2}\right)\\
&-2\left((k-2)(k-3)(6+(k+5)l)\kappa_1^0 es_{k-l}+(k+2)(k+3)(6-(k-5)l)\kappa_1^0 es_{k+l}\right)\\
&+(k-1)(k-2)(k-3)\left((l-1)\kappa_1^0 es_{k-l+2}+(l+1)\kappa_1^0 es_{k+l+2}\right)\\
&-120\sum_{j=0}^{l}(k+2j-l)\kappa_1^0 es_{k+2j-l}\Bigg]
\end{aligned}
\tag{B.1c}
$$

$$
\begin{aligned}
k_{14}(k,l)=&+\frac{1}{2}\Big((k+1)(k+2)(k+3)\left(\kappa_1^1 es_{k-l-4}+\kappa_1^1 es_{k+l-4}\right)-4(k+3)\left(k^2-4\right)\left(\kappa_1^1 es_{k-l-2}+\kappa_1^1 es_{k+l-2}\right)\\
&+6k\left(k^2-9\right)\left(\kappa_1^1 es_{k-l}+\kappa_1^1 es_{k+l}\right)-4(k-3)\left(k^2-4\right)\left(\kappa_1^1 es_{k-l+2}+\kappa_1^1 es_{k+l+2}\right)\\
&+(k-1)(k-2)(k-3)\left(\kappa_1^1 es_{k-l+4}+\kappa_1^1 es_{k+l+4}\right)\Big)
\end{aligned}
\tag{B.1d}
$$

$$
\begin{aligned}
k_{21}(k,l)=&\,dl\Big((k+1)(k+2)(k+3)\left(\kappa^1 a_{k-l-3}-\kappa^1 a_{k+l-3}\right)-3(k+2)\left(k^2-9\right)\left(\kappa^1 a_{k-l-1}-\kappa^1 a_{k+l-1}\right)\\
&+3(k-2)\left(k^2-9\right)\left(\kappa^1 a_{k-l+1}-\kappa^1 a_{k+l+1}\right)+(k-1)(k-2)(k-3)\left(\kappa^1 a_{k-l+3}-\kappa^1 a_{k+l+3}\right)\Big)\\
&-2\left(k^2-9\right)\left(k^2-4\right)\Big((k+1)\left(\kappa_1^0 el_{k-l-2}+\kappa_1^0 el_{k+l-2}\right)\\
&-2k\left(\kappa_1^0 el_{k-l}+\kappa_1^0 el_{k+l}\right)+(k-1)\left(\kappa_1^0 el_{k-l+2}+\kappa_1^0 el_{k+l+2}\right)\Big)\\
&-\frac{1}{2}\Big((k+1)(k+2)(k+3)\left(\kappa_1^2 el_{k-l-4}+\kappa_1^2 el_{k+l-4}\right)-4(k+3)\left(k^2-4\right)\left(\kappa_1^2 el_{k-l-2}+\kappa_1^2 el_{k+l-2}\right)\\
&+6k\left(k^2-9\right)\left(\kappa_1^2 el_{k-l}+\kappa_1^2 el_{k+l}\right)-4(k-3)\left(k^2-4\right)\left(\kappa_1^2 el_{k-l+2}+\kappa_1^2 el_{k+l+2}\right)\\
&+(k-1)(k-2)(k-3)\left(\kappa_1^2 el_{k-l+4}+\kappa_1^2 el_{k+l+4}\right)\Big)
\end{aligned}
\tag{B.1e}
$$

$$
\begin{aligned}
k_{22}(k,l)=&-8l\left(k^2-9\right)\left(k^2-4\right)\Bigg((k-1)(l+1)el_{k-l}-2\sum_{j=0}^{l}(k+2j-l)el_{k+2j-l}+(k+1)(l+1)el_{k+l}\Bigg)\\
&-2\Bigg((k+1)(k+2)(k+3)\left((k(k-5)+6+l(l-1))\kappa_0^2 el_{k-l-2}+(k(k-5)+6+l(l+1))\kappa_0^2 el_{k+l-2}\right)\\
&-2(k-2)(k-3)(k(k+2)(k+3)+6l+l^2(k+5)\kappa_0^2 el_{k-l}
\end{aligned}
$$

$$
\begin{aligned}
&-2(k+2)(k+3)(k(k-2)(k-3)-6l+l^2(k-5)\kappa_0^2 el_{k+l} \\
&+(k-1)(k-2)(k-3)\left((k(k+5)+6+l(l+1))\kappa_0^2 el_{k-l-2}+(k(k+5)+6+l(l-1))\kappa_0^2 el_{k+l-2}\right) \\
&-120l\sum_{j=0}^{l}(k+2j-l)\kappa_0^2 el_{k+2j-l}\Bigg) \\
&-\frac{1}{2}d\Big((k+1)(k+2)(k+3)\left(\kappa_0^2 a_{k-l-4}+\kappa_0^2 a_{k+l-4}\right)-4(k+3)\left(k^2-4\right)\left(\kappa^2 a_{k-l-2}+\kappa^2 a_{k+l-2}\right) \\
&+6k\left(k^2-9\right)\left(\kappa^2 a_{k-l}+\kappa^2 a_{k+l}\right)-4(k-3)\left(k^2-4\right)\left(\kappa^2 a_{k-l+2}+\kappa^2 a_{k+l+2}\right) \\
&+(k-1)(k-2)(k-3)\left(\kappa^2 a_{k-l+4}+\kappa^2 a_{k+l+4}\right)\Big) \\
&-\frac{1}{2}\Big((k+1)(k+2)(k+3)\left(\kappa_0^4 el_{k-l-4}+\kappa_0^4 el_{k+l-4}\right)-4(k+3)\left(k^2-4\right)\left(\kappa_0^4 el_{k-l-2}+\kappa_0^4 el_{k+l-2}\right) \\
&+6k\left(k^2-9\right)\left(\kappa_0^4 el_{k-l}+\kappa_0^4 el_{k+l}\right)-4(k-3)\left(k^2-4\right)\left(\kappa_0^4 el_{k-l+2}+\kappa_0^4 el_{k+l+2}\right) \\
&+(k-1)(k-2)(k-3)\left(\kappa_0^4 el_{k-l+4}+\kappa_0^4 el_{k+l+4}\right)\Big)
\end{aligned}
\tag{B.1f}
$$

$$
\begin{aligned}
k_{23}(k,l) = &-8l\left(k^2-9\right)\left(k^2-4\right)\left((k-1)(l+1)es_{k-l}-2\sum_{j=0}^{l}(k+2j-l)es_{k+2j-l}+(k+1)(l+1)es_{k+l}\right) \\
&-2l\Bigg[(k+1)(k+2)(k+3)\left((l-1)\kappa_0^2 es_{k-l-2}+(l+1)\kappa_0^2 es_{k+l-2}\right) \\
&-2\left((k-2)(k-3)(6+(k+5)l)\kappa_0^2 es_{k-l}+(k+2)(k+3)(6-(k-5)l)\kappa_0^2 es_{k+l}\right) \\
&+(k-1)(k-2)(k-3)\left((l-1)\kappa_0^2 es_{k-l+2}+(l+1)\kappa_0^2 es_{k+l+2}\right) \\
&-120\sum_{j=0}^{l}(k+2j-l)\kappa_0^2 es_{k+2j-l}\Bigg]
\end{aligned}
\tag{B.1g}
$$

$$
\begin{aligned}
k_{24}(k,l) = &\,2\left(k^2-9\right)\left(k^2-4\right)\Big((k+1)\left(\kappa_0^1 es_{k-l-2}+\kappa_0^1 es_{k+l-2}\right) \\
&-2k\left(\kappa_0^1 es_{k-l}+\kappa_0^1 es_{k+l}\right)+(k-1)\left(\kappa_0^1 es_{k-l+2}+\kappa_0^1 es_{k+l+2}\right)\Big) \\
&+\frac{1}{2}\Big((k+1)(k+2)(k+3)\left(\kappa_0^3 es_{k-l-4}+\kappa_0^3 es_{k+l-4}\right)-4(k+3)\left(k^2-4\right)\left(\kappa_0^3 es_{k-l-2}+\kappa_0^3 es_{k+l-2}\right) \\
&+6k\left(k^2-9\right)\left(\kappa_0^3 es_{k-l}+\kappa_0^3 es_{k+l}\right)-4(k-3)\left(k^2-4\right)\left(\kappa_0^3 es_{k-l+2}+\kappa_0^3 es_{k+l+2}\right) \\
&+(k-1)(k-2)(k-3)\left(\kappa_0^3 es_{k-l+4}+\kappa_0^3 es_{k+l+4}\right)\Big)
\end{aligned}
\tag{B.1h}
$$

$$
\begin{aligned}
k_{31}(k,l) = &-2\left(k^2-9\right)\left(k^2-4\right)\Big((k+1)\left(\kappa_1^0 es_{k-l-2}+\kappa_1^0 es_{k+l-2}\right) \\
&-2k\left(\kappa_1^0 es_{k-l}+\kappa_1^0 es_{k+l}\right)+(k-1)\left(\kappa_1^0 es_{k-l+2}+\kappa_1^0 es_{k+l+2}\right)\Big)
\end{aligned}
\tag{B.1i}
$$

$$
\begin{aligned}
k_{32}(k,l) = &-8\left(k^2-9\right)\left(k^2-4\right)l\left((l+1)\left((k-1)es_{k-l}+(k+1)es_{k+l}\right)-2\sum_{j=0}^{l}(k+2j-l)es_{k+2j-l}\right) \\
&+2l\left(k^2-9\right)\Big((k+1)(k+2)\left(\kappa^2 es_{k-l-2}-\kappa^2 es_{k+l-2}\right)-2\left(k^2-4\right)\left(\kappa^2 es_{k-l}-\kappa^2 es_{k+l}\right) \\
&+(k-1)(k-2)\left(\kappa^2 es_{k-l-2}-\kappa^2 es_{k+l-2}\right)\Big)
\end{aligned}
\tag{B.1j}
$$

$$\begin{aligned}
k_{33}(k,l) = & -8\left(k^2-9\right)\left(k^2-4\right)l\left((l+1)\left((k-1)\,ed_{k-l}+(k+1)\,ed_{k+l}\right)-2\sum_{j=0}^{l}(k+2j-l)\,ed_{k+2j-l}\right) \\
& +2l\left(k^2-9\right)\left((k+1)(k+2)\left(\kappa^2 g_{k-l-2}-\kappa^2 g_{k+l-2}\right)-2\left(k^2-4\right)\left(\kappa^2 g_{k-l}-\kappa^2 g_{k+l}\right)\right. \\
& \left.+(k-1)(k-2)\left(\kappa^2 g_{k-l-2}-\kappa^2 g_{k+l-2}\right)\right)
\end{aligned} \tag{B.1k}$$

$$\begin{aligned}
k_{34}(k,l) = & 2l\left(k^2-9\right)\left((k+1)(k+2)\left(\kappa^1 g_{k-l-2}-\kappa^1 g_{k+l-2}\right)-2\left(k^2-4\right)\left(\kappa^1 g_{k-l}-\kappa^1 g_{k+l}\right)\right. \\
& \left.+(k-1)(k-2)\left(\kappa^1 g_{k-l+2}-\kappa^1 g_{k+l+2}\right)\right) \\
& +2\left(k^2-9\right)\left(k^2-4\right)\left((k+1)\left(\kappa^1 ed_{k-l-2}+\kappa^1 ed_{k+l-2}\right)-2k\left(\kappa^1 ed_{k-l}+\kappa^1 ed_{k+l}\right)\right. \\
& \left.+(k-1)\left(\kappa^1 ed_{k-l+2}+\kappa^1 ed_{k+l+2}\right)\right)
\end{aligned} \tag{B.1l}$$

$$\begin{aligned}
k_{41}(k,l) = & +\frac{1}{2}\left((k+1)(k+2)(k+3)\left(\kappa_1^1 es_{k-l-4}+\kappa_1^1 es_{k+l-4}\right)-4(k+3)\left(k^2-4\right)\left(\kappa_1^1 es_{k-l-2}+\kappa_1^1 es_{k+l-2}\right)\right. \\
& +6k\left(k^2-9\right)\left(\kappa_1^1 es_{k-l}+\kappa_1^1 es_{k+l}\right)-4(k-3)\left(k^2-4\right)\left(\kappa_1^1 es_{k-l+2}+\kappa_1^1 es_{k+l+2}\right) \\
& \left.+(k-1)(k-2)(k-3)\left(\kappa_1^1 es_{k-l+4}+\kappa_1^1 es_{k+l+4}\right)\right)
\end{aligned} \tag{B.1m}$$

$$\begin{aligned}
k_{42}(k,l) = & -2l\left[(k+1)(k+2)(k+3)\left((l-1)\,\kappa_0^1 es_{k-l-2}+(l+1)\,\kappa_0^1 es_{k+l-2}\right)\right. \\
& -2\left((k-2)(k-3)(6+(k+5)\,l)\,\kappa_0^1 es_{k-l}+(k+2)(k+3)(6-(k-5)\,l)\,\kappa_0^1 es_{k+l}\right) \\
& +(k-1)(k-2)(k-3)\left((l-1)\,\kappa_0^1 es_{k-l+2}+(l+1)\,\kappa_0^1 es_{k+l+2}\right) \\
& \left.-120\sum_{j=0}^{l}(k+2j-l)\,\kappa_0^1 es_{k+2j-l}\right]
\end{aligned} \tag{B.1n}$$

$$\begin{aligned}
k_{43}(k,l) = & 2l\left((k+1)(k+2)(k+3)\left((l-1)\,\kappa^1 ed_{k-l-2}+(l+1)\,\kappa^1 ed_{k+l-2}\right)\right. \\
& -\left(2(k-2)(k-3)((k+5)\,l+6)\,\kappa^1 ed_{k-l}+2(k+2)(k+3)((k-5)\,l-6)\,\kappa^1 ed_{k+l}\right) \\
& \left.+(k-1)(k-2)(k-3)\left((l+1)\,\kappa^1 ed_{k-l+2}+(l-1)\,\kappa^1 ed_{k+l+2}\right)-120\sum_{j=0}^{l}(k+2j-l)\,\kappa^1 ed_{k+2j-l}\right) \\
& -2l\left(k^2-9\right)\left((k+1)(k+2)\left(\kappa^1 g_{k-l-2}-\kappa^1 g_{k+l-2}\right)-2\left(k^2-4\right)\left(\kappa^1 g_{k-l}-\kappa^1 g_{k+l}\right)\right. \\
& \left.+(k-1)(k-2)\left(\kappa^1 g_{k-l+2}-\kappa^1 g_{k+l+2}\right)\right)
\end{aligned} \tag{B.1o}$$

$$\begin{aligned}
k_{44}(k,l) = & 2l\left(k^2-9\right)\left((k+1)(k+2)\left(g_{k-l-2}-g_{k+l+2}\right)\right. \\
& \left.-2\left(k^2-4\right)\left(g_{k-l}-g_{k+l}\right)+(k-1)(k-2)\left(g_{k-l+2}-g_{k+l+2}\right)\right) \\
& -\frac{1}{2}\left((k+1)(k+2)(k+3)\left(\kappa^2 ed_{k-l-4}+\kappa^2 ed_{k+l-4}\right)-4(k+3)\left(k^2-4\right)\left(\kappa^2 ed_{k-l-2}+\kappa^2 ed_{k+l-2}\right)\right. \\
& +6k\left(k^2-9\right)\left(\kappa^2 ed_{k-l}+\kappa^2 ed_{k+l}\right)-4(k-3)\left(k^2-4\right)\left(\kappa^2 ed_{k-l+2}+\kappa^2 ed_{k+l+2}\right) \\
& \left.+(k-1)(k-2)(k-3)\left(\kappa^2 ed_{k-l+4}+\kappa^2 ed_{k+l+4}\right)\right)
\end{aligned} \tag{B.1p}$$

$$
\begin{aligned}
b_{11}(k,l) &= b_{22}(k,l) = b_{33}(k,l) \\
&= \frac{1}{2} g \Big((k+1)(k+2)(k+3)\left(\rho_{k-l-4}+\rho_{k+l-4}\right) - 4\left(k^2-4\right)(k+3)\left(k^2-4\right)\left(\rho_{k-l-2}+\rho_{k+l-2}\right) \\
&\quad + 6k\left(k^2-9\right)\left(\rho_{k-l}+\rho_{k+l}\right) - 4\left(k^2-4\right)(k-3)\left(k^2-4\right)\left(\rho_{k-l+2}+\rho_{k+l+2}\right) \\
&\quad + (k-1)(k-2)(k-3)\left(\rho_{k-l+4}+\rho_{k+l+4}\right)\Big) \qquad \text{(B.2)} \\
b_{44}(k,l) &= \frac{1}{2} g \Big((k+1)(k+2)(k+3)\left(i_{k-l-4}+i_{k+l-4}\right) - 4\left(k^2-4\right)(k+3)\left(k^2-4\right)\left(i_{k-l-2}+i_{k+l-2}\right) \\
&\quad + 6k\left(k^2-9\right)\left(i_{k-l}+i_{k+l}\right) - 4\left(k^2-4\right)(k-3)\left(k^2-4\right)\left(i_{k-l+2}+i_{k+l+2}\right) \\
&\quad + (k-1)(k-2)(k-3)\left(i_{k-l+4}+i_{k+l+4}\right)\Big) \\
P_1(k,l) &= -f\Big((k+1)(k+2)(k+3)\,p_{k-4} - 4(k+3)\left(k^2-4\right)p_{k-2} \\
&\quad + 6k\left(k^2-9\right)p_k - 4(k-3)\left(k^2-4\right)p_{k+2} + (k-1)(k-2)(k-3)\,p_{k+4}\Big) \\
&\quad - \Big((k+1)(k+2)(k+3)\,\kappa m_{k-4} - 4(k+3)\left(k^2-4\right)\kappa m_{k-2} \\
&\quad + 6k\left(k^2-9\right)\kappa m_k - 4(k-3)\left(k^2-4\right)\kappa m_{k+2} + (k-1)(k-2)(k-3)\,\kappa m_{k+4}\Big), \\
P_2(k,l) &= -f\Big((k+1)(k+2)(k+3)\,r_{k-4} - 4(k+3)\left(k^2-4\right)r_{k-2} \\
&\quad + 6k\left(k^2-9\right)r_k - 4(k-3)\left(k^2-4\right)r_{k+2} + (k-1)(k-2)(k-3)\,r_{k+4}\Big) \\
&\quad - \left(k^2-9\right)\Big((k+1)(k+2)\,\kappa m_{k-3} - 3(k-1)(k+2)\left(k^2-4\right)\kappa m_{k-1} \\
&\quad + 3(k+1)(k-2)\,\kappa m_{k+1} - (k-1)(k-2)\,\kappa m_{k+3}\Big), \qquad \text{(B.3)} \\
P_3(k,l) &= -f\Big((k+1)(k+2)(k+3)\,q_{k-4} - 4(k+3)\left(k^2-4\right)q_{k-2} \\
&\quad + 6k\left(k^2-9\right)q_k - 4(k-3)\left(k^2-4\right)q_{k+2} + (k-1)(k-2)(k-3)\,q_{k+4}\Big) \\
&\quad - \left(k^2-9\right)\Big((k+1)(k+2)\,n_{k-3} - 3(k-1)(k+2)\left(k^2-4\right)n_{k-1} \\
&\quad + 3(k+1)(k-2)\,n_{k+1} - (k-1)(k-2)\,n_{k+3}\Big), \\
P_4(k,l) &= -f\Big((k+1)(k+2)(k+3)\,t_{k-4} - 4(k+3)\left(k^2-4\right)t_{k-2} \\
&\quad + 6k\left(k^2-9\right)t_k - 4(k-3)\left(k^2-4\right)t_{k+2} + (k-1)(k-2)(k-3)\,t_{k+4}\Big),
\end{aligned}
$$

where the coefficients in formulas (B.1a)–(B.3) are the coefficients of expansion of the following functions into a Chebyshev series:

$$
\begin{aligned}
&ed_l = a_l\left[EI_y\right], \quad \kappa^p ed_l = a_l\left[\kappa^p EI_y\right], \\
&el_l = a_l\left[EI_z\right], \quad \kappa_q^p el_l = a_l\left[\left(\kappa^{(1)}\right)^q \kappa^p EI_z\right], \\
&es_l = a_l\left[EI_{yz}\right], \quad \kappa_q^p es_l = a_l\left[\left(\kappa^{(1)}\right)^q \kappa^p EI_{yz}\right], \\
&a_l = a_l\left[EA\right], \quad \kappa^p a_l = a_l\left[\kappa^p EA\right], \\
&g_l = a_l\left[GJ_s\right], \quad \kappa^p g_l = a_l\left[\kappa^p GJ_s\right], \\
&\rho_l = a_l\left[\rho\right], \quad i_l = a_l\left[J_s^m\right], \\
&p_l = a_l\left[p_x\right], \quad r_l = a_l\left[p_y\right], \quad q_l = a_l\left[q_z\right], \\
&t_l = a_l\left[m_x\right], \quad n_l = a_l\left[m_y\right], \quad m_l = a_l\left[m_z\right], \\
&\kappa m_l = a_l\left[\kappa m_z\right].
\end{aligned} \qquad \text{(B.4)}
$$

C. Reduction of Matrix to Jordan Canonical Form

In the paper the following theorem is used.

Theorem C.1. *For each square matrix* **A** *of n degree there exists nonsingular matrix* **S** *reducing matrix* **A** *to a certain matrix*

$$\mathbf{J} = \mathbf{SAS}^{-1}, \quad (\det \mathbf{S} \neq 0) \qquad \text{(C.1)}$$

having this Jordan form

$$\mathbf{J} = \operatorname{diag}\left[\mathbf{J}_1(\lambda_1), \mathbf{J}_2(\lambda_2), \ldots, \mathbf{J}_m(\lambda_m)\right], \quad m \le n, \tag{C.2}$$

where $\lambda_1, \lambda_2, \ldots, \lambda_m$ *are different eigenvalues of matrix* $\mathbf{A}$,

$$\mathbf{J}_k(\lambda_k) = \operatorname{diag}\left[\mathbf{J}_k^{(1)}(\lambda_k), \mathbf{J}_k^{(2)}(\lambda_k), \ldots, \mathbf{J}_k^{(r)}(\lambda_k)\right], \quad r = r(k), \tag{C.3}$$

$$\mathbf{J}_k^{(i)}(\lambda_k) = \begin{bmatrix} \lambda_k & 1 & 0 & \ldots & 0 \\ 0 & \lambda_k & 1 & \ldots & 0 \\ \ldots & \ldots & \ldots & \ldots & \ldots \\ 0 & 0 & 0 & \ldots & 1 \\ 0 & 0 & 0 & \ldots & \lambda_k \end{bmatrix}, \tag{C.4}$$

$$i = 1, 2, \ldots, r(k), \; k = 1, 2, \ldots, m, \; \dim\left[\mathbf{J}_k^{(i)}(\lambda_k)\right] = e_k^{(i)} \times e_k^{(i)}$$

is the so-called Jordan cage corresponding to eigenvalue λ_k, *with one or several Jordan cages of* $e_k^{(i)}$ *degree, where* $e_k^{(1)} + e_k^{(2)} + \cdots + e_k^{(r)} = \alpha_k$, $r = r(k)$, $k = 1, 2, \ldots, m$, *and* $\alpha_1 + \alpha_2 + \cdots + \alpha_m = n$, *corresponding to each eigenvalue* λ_k *of matrix* $\mathbf{A}$, *with multiplicity* α_k.

In a special case when all the eigenvalues of matrix $\mathbf{A}$ are single, all the Jordan cages corresponding to λ_k get reduced to simple one-element cages $\mathbf{J}_k^{(i)}(\lambda_k) = [\lambda_k]$. In the considered case

$$\mathbf{J} = \{\lambda\} = \operatorname{diag}\left[\lambda_1, \lambda_2, \ldots, \lambda_n\right], \tag{C.5}$$

and transformation matrix $\mathbf{S} = \mathbf{W}^{-1}$ is the inverse of eigenmatrix $\mathbf{W}$, i.e., a matrix satisfying the equation $\mathbf{AW} = \mathbf{W}\{\lambda\}$.

Data Availability

No data were used to support this study.

Conflicts of Interest

The authors declare that there are no conflicts of interest regarding the publication of this paper.

References

[1] G. R. Liu and T. Y. Wu, "In-plane vibration analyses of circular arches by the generalized differential quadrature rule," *International Journal of Mechanical Sciences*, vol. 43, no. 11, pp. 2597–2611, 2001.

[2] P. Chidamparam and A. W. Leissa, "Influence of centerline extensibility on the in-plane free vibrations of loaded circular arches," *Journal of Sound and Vibration*, vol. 183, no. 5, pp. 779–795, 1995.

[3] S.-Y. Lee, J.-J. Sheu, and S.-M. Lin, "In-plane vibrational analysis of rotating curved beam with elastically restrained root," *Journal of Sound and Vibration*, vol. 315, no. 4-5, pp. 1086–1102, 2008.

[4] C. S. Huang, Y. P. Tseng, A. W. Leissa, and K. Y. Nieh, "An exact solution for in-plane vibrations of an arch having variable curvature and cross section," *International Journal of Mechanical Sciences*, vol. 40, no. 11, pp. 1159–1173, 1998.

[5] M. Kawakami, T. Sakiyama, H. Matsuda, and C. Morita, "In-plane and out-of-plane free vibrations of curved beams with variable sections," *Journal of Sound and Vibration*, vol. 187, no. 3, pp. 381–401, 1995.

[6] Y.-J. Shin, K.-M. Kwon, and J.-H. Yun, "Vibration analysis of a circular arch with variable cross-section using differential transformation and generalized differential quadrature," *Journal of Sound and Vibration*, vol. 309, no. 1-2, pp. 9–19, 2008.

[7] X. Tong, N. Mrad, and B. Tabarrok, "In-plane vibration of circular arches with variable cross-sections," *Journal of Sound and Vibration*, vol. 212, no. 1, pp. 121–140, 1998.

[8] C. S. Huang, K. Y. Nieh, and M. C. Yang, "In-plane free vibration and stability of loaded and shear-deformable circular arches," *International Journal of Solids and Structures*, vol. 40, no. 22, pp. 5865–5886, 2003.

[9] G. Karami and P. Malekzadeh, "In-plane free vibration analysis of circular arches with varying cross-sections using differential quadrature method," *Journal of Sound and Vibration*, vol. 274, no. 3-5, pp. 777–799, 2004.

[10] K. Y. Nieh, C. S. Huang, and Y. P. Tseng, "An analytical solution for in-plane free vibration and stability of loaded elliptic arches," *Computers & Structures*, vol. 81, no. 13, pp. 1311–1327, 2003.

[11] S. A. Eftekhari, "Differential quadrature procedure for in-plane vibration analysis of variable thickness circular arches traversed by a moving point load," *Applied Mathematical Modelling*, vol. 40, no. 7-8, pp. 4640–4663, 2016.

[12] A. Krishnan, S. Dharmaraj, and Y. Suresh, "Free vibration studies of arches," *Journal of Sound and Vibration*, vol. 186, no. 5, pp. 856–863, 1995.

[13] P. Raveendranath, G. Singh, and B. Pradhan, "Free vibration of arches using a curved beam element based on a coupled polynomial displacement field," *Computers & Structures*, vol. 78, no. 4, pp. 583–590, 2000.

[14] F. Yang, R. Sedaghati, and E. Esmailzadeh, "Free in-plane vibration of general curved beams using finite element method," *Journal of Sound and Vibration*, vol. 318, no. 4-5, pp. 850–867, 2008.

[15] H. Öztürk, I. Yeşilyurt, and M. Sabuncu, "In-plane stability analysis of non-uniform cross-sectioned curved beams," *Journal of Sound and Vibration*, vol. 296, no. 1-2, pp. 277–291, 2006.

[16] P. Litewka and J. Rakowski, "An efficient curved beam finite element," *International Journal for Numerical Methods in Engineering*, vol. 40, no. 14, pp. 2629–2652, 1997.

[17] P. Litewka and J. Rakowski, "Free vibration of shear-flexible and compressible arches by FEM," *International Journal for Numerical Methods in Engineering*, vol. 52, no. 3, pp. 273–286, 2001.

[18] Z. H. Zhu and S. A. Meguid, "Vibration analysis of a new curved beam element," *Journal of Sound and Vibration*, vol. 309, no. 1-2, pp. 86–95, 2008.

[19] B. Kang, C. H. Riedel, and C. A. Tan, "Free vibration analysis of planar curved beams by wave propagation," *Journal of Sound and Vibration*, vol. 260, no. 1, pp. 19–44, 2003.

[20] C. H. Riedel and B. Kang, "Free vibration of elastically coupled dual-span curved beams," *Journal of Sound and Vibration*, vol. 290, no. 3-5, pp. 820–838, 2006.

[21] M. Ishaquddin, P. Raveendranath, and J. N. Reddy, "Efficient coupled polynomial interpolation scheme for out-of-plane free vibration analysis of curved beams," *Finite Elements in Analysis and Design*, 2014.

[22] R.-A. Jafari-Talookolaei, M. Abedi, and M. Hajianmaleki, "Vibration characteristics of generally laminated composite curved beams with single through-the-width delamination," *Composite Structures*, vol. 138, pp. 172–183, 2016.

[23] X. Li and C. Guedes Soares, "Spectral finite element analysis of in-plane free vibration of laminated composite shallow arches," *Composite Structures*, vol. 132, pp. 484–494, 2015.

[24] T. Ye, G. Jin, and Z. Su, "A spectral-sampling surface method for the vibration of 2-D laminated curved beams with variable curvatures and general restraints," *International Journal of Mechanical Sciences*, vol. 110, pp. 170–189, 2016.

[25] E. Sadeghpour, M. Sadighi, and A. Ohadi, "Free vibration analysis of a debonded curved sandwich beam," *European Journal of Mechanics - A/Solids*, vol. 57, pp. 71–84, 2016.

[26] A. M. Yu, C. J. Yang, and G. H. Nie, "Analytical formulation and evaluation for free vibration of naturally curved and twisted beams," *Journal of Sound and Vibration*, vol. 329, no. 9, pp. 1376–1389, 2010.

[27] I. Caliò, A. Greco, and D. D'Urso, "Free vibrations of spatial Timoshenko arches," *Journal of Sound and Vibration*, vol. 333, no. 19, pp. 4543–4561, 2014.

[28] N. M. Auciello and M. A. De Rosa, "Free vibrations of circular arches: a review," *Journal of Sound and Vibration*, vol. 176, no. 4, pp. 433–458, 1994.

[29] P. Ruta, "Application of Chebyshev series to solution of non-prismatic beam vibration problems," *Journal of Sound and Vibration*, vol. 227, no. 2, pp. 449–467, 1999.

[30] P. Ruta, "Dynamic stability problem of a non-prismatic rod," *Journal of Sound and Vibration*, vol. 250, no. 3, pp. 445–464, 2002.

[31] P. Ruta, "The application of Chebyshev polynomials to the solution of the nonprismatic Timoshenko beam vibration problem," *Journal of Sound and Vibration*, vol. 296, no. 1-2, pp. 243–263, 2006.

[32] S. Paszkowski, *Zastosowania numeryczne wielomianów Czebyszewa (*Numerical applications of Chebyshev polynomials*)*, Państwowe Wydawnictwo Naukowe, 1975.

[33] M. Kleiber and M. Edited by, Eds., "Komputerowe metody, mechaniki cial stalych (Computer methods for solid body mechanics," Tech. Rep., Warsaw, 1995.

[34] Wolfram Research, Inc., Mathematica, Version 7.0, Champaign, IL (2008).